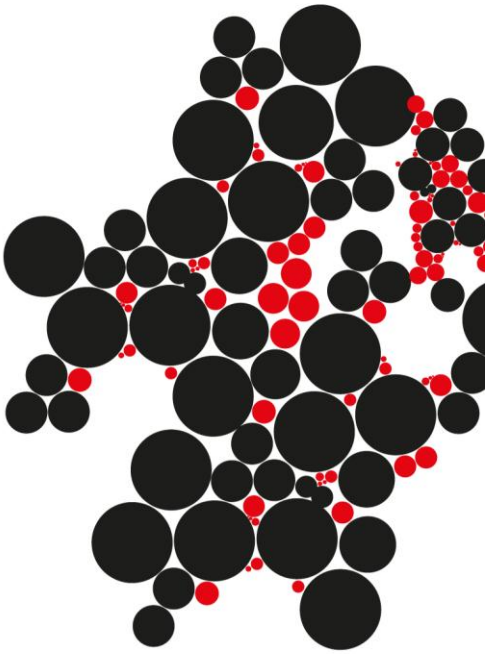

MODELLING ASPHALT WITH DISCRETE AND CONTINUUM METHODS

T.J. Ormel

MECHANICAL ENGINEERING
CHAIR OF APPLIED MECHANICS

EXAMINATION COMMITTEE
Dr. Ir. A.H. van den Boogaard
Prof. Dr. rer.-nat. S. Luding
Dr. Ir. V.T. Meinders
M. Sc. C. Wang

DOCUMENT NUMBER
CTW.12 – TM-5692
MSM-005
TRC-001

UNIVERSITY OF TWENTE.

14-8-2012

ABSTRACT

Asphalt is used in many pavement constructions. During pavement construction the asphalt is compacted; this process is critical for obtaining a high quality, long-lasting pavement. Knowledge about the compaction process is mainly based on the results of experimental and empirical investigation. The use of numerical models, capable of describing the behaviour of asphalt during compaction, could lead to a better understanding of the compaction process and contribute to the constructing of better roads. Unfortunately, limited research has been performed on numerical modelling of asphalt compaction and a fundamental micro-based model, able to describe the particle behaviour during compaction, is not available. The complexity of the asphalt material and the many factors that can influence compaction, greatly complicate efforts to develop numerical models. In this research a numerical model, based on the discrete element method (DEM), capable of modelling a simplified method of compaction is developed. This model is appropriate for modelling the behaviour of particles on the meso-scale, which means that the behaviour of an assembly of particles can be modelled during compaction using micro-based parameters. Model parameters are calibrated by performing experimental compaction tests on actual asphalt mixtures. Model- and experimental results are compared in stress-strain relations. A good match between DEM- and experimental results is obtained. However, the DEM model is not capable for modelling the total road behaviour on the macro-scale. Therefore, this research tries to bridge the gap between the micro- and macro-scale, by linking the DEM model to a material model available in Abaqus (Finite Element Program), which can be applied on the macro-scale. Calibration of the material model is performed with the use of DEM simulations. In this way a macro-scale model using micro-based parameters is obtained.

SAMENVATTING

Asfalt wordt gebruikt in tal van bestrating constructies. Tijdens de constructie van wegen wordt het asfalt mengsel verdicht, dit proces is van cruciaal belang voor het verkrijgen van een duurzame bestrating van hoge kwaliteit. Kennis over het verdichtingsproces is voornamelijk gebaseerd op de resultaten van experimenteel en empirisch onderzoek. Het gebruik van numerieke modellen die in staat zijn het gedrag van asfalt materiaal tijdens verdichting te beschrijven, zouden kunnen leiden tot het beter begrijpen van het verdichtingsproces en bijdragen aan het construeren van betere wegen. Helaas is weinig onderzoek gedaan op het gebied van numerieke modellering van asfalt verdichting en een fundamentele micro-schalig model dat in staat is het gedrag van deeltjes te beschrijven tijdens compactie is niet beschikbaar. De complexiteit van het asfalt materiaal en de vele factoren die van invloed kunnen zijn op het verdichtingsproces, compliceren poginggen om numerieke modellen te ontwikkelen. In dit onderzoek is een numeriek model ontwikkeld, gebaseerd op de discrete elementen methode (DEM), voor het modelleren van een vereenvoudigde wijze van verdichting. Dit model is geschikt voor het modelleren van het deeltjes gedrag op de meso-schaal, wat betekent dat het gedrag van een verzameling deeltjes gemodelleerd kan worden tijdens compactie, met behulp van micro-schalige model parameters. Model parameters worden gekalibreerd door het uitvoeren experimentele verdichtings testen van werkelijk asfalt. Model-en experimentele resultaten worden vergeleken in spanning-rek relaties. Een goede overeenkomst tussen DEM- en experimentele resultaten is verkregen. Echter, het DEM model is niet in staat om het totale weg gedrag op de macro-schaal te modelleren. Daarom is in dit onderzoek getracht een brug te slaan tussen de micro-en macro-schaal, door het koppelen van DEM aan een materiaal model beschikbaar in Abaqus (Eindig Elementen Programma). Kalibratie van het materiaal model is uitgevoerd met gebruik van de DEM simulaties. Op deze wijze wordt een macro-schaalmodel, gebaseerd op micro-schalige parameters verkregen.

PREFACE

This thesis is made as a completion of my master program Mechanical Engineering at the faculty Engineering Technology of the University of Twente. During the period (October 2011 till August 2012) I enjoyed working on my master assignment. It was a joint project between two groups from the Mechanical Engineering department: Applied Mechanics (my own group) and Multi-scale Mechanics and also the Civil Engineering department was involved.

I am grateful for the practical and academical support of several persons. I would in particular thank my supervisor Ton van den Boogaard, my co-supervisors Vanessa Magnanimo, Stefan Luding and Henny ter Huerne for their valuable input and support throughout my assignment. I would also like to thank the employees of Reef Infra B.V., who assisted with the experimental tests. I hope that readers will find enjoyment in taking note of the content of this thesis.

Tom Ormel
Enschede, 14-8-2012

CONTENTS

1 INTRODUCTION

In this chapter the research is introduced. First, asphalt material and compaction are explained, followed by a short overview of different modelling approaches regarding asphalt. Then, research description and research goals are described. The chapter concludes with the outline of the thesis.

1.1 ASPHALT AND COMPACTION

Asphalt is used in many pavement constructions. It is a multiphase material consisting of different sized aggregates, viscous bitumen, sand, fillers and air voids. It can be considered in two different states: (1) hot and non-compacted, during the construction phase and (2) compacted at ambient temperature, during the lifetime of a road. During pavement construction the asphalt mixture is in the hot non-compacted state and placed on a hardened foundation. Subsequently, the compaction is started, usually by moving heavy weighted rollers over the asphalt. This forces aggregates together, which achieves stability and provides resistance to deformation, while simultaneously densifying the material and improving its durability. After compaction and cooling down, the asphalt should be capable of carrying loads for a specifically designed life-time.

Obviously, road failure phenomena like rutting or wearing (see Figure 1) are undesirable, but can nevertheless occur for many reasons, for example inadequate compaction. When after compaction the desired density, on which the strength of the pavement depends, is not reached, then rutting can occur in an early stage due to traffic loads. The compaction process is critical in obtaining a high quality, long-lasting asphalt pavement. Poorly compacted pavements just do not meet expectations, which is unacceptable in an environment where the costs of materials and construction are at all-time heights. It is therefore essential to fully understand the compaction process. This knowledge is mainly based on experimental and empirical investigation. If available, numerical models which simulate asphalt compaction could be used in a predictive manner to help construct better roads,

Figure 1: Examples of rutting (left) and cracking (right)

which may save costs and time. Unfortunately, limited research has been done in micro-scale, or multi-scale based numerical modelling of asphalt compaction. The complexity of the asphalt material and the many factors that can influence compaction, greatly complicate efforts to develop numerical models.

When considering asphalt, it makes sense to distinguish between different length scales, i.e. the micro-, meso- and macro-scale. The interaction between the mastic (composed of bitumen and fine mineral particles) and a single stone of the aggregate is defined as the micro-scale; the meso-scale is defined as the interaction between multiple stones of various sizes and the mastic, while the macro-scale describes the entire road behaviour. The kinematics on these different scales apparently control the behaviour of the material. To gain a thorough understanding of the behaviour of asphalt pavements, one has to consider all length scales. In the professional asphalt branch fundamental constitutive models, capable of describing the micro- and meso-mechanical behaviour, are hardly used. Macro-scale problems like rutting, raveling and cracking are studied by applying empirical models, which give only limited insight into the micro-scale behaviour. This research tried to bridge the gap between the micro- and macro-scale, by finding and calibrating a model, suitable for modelling the meso-scale behaviour of particles, using micro-based parameters, with predictive qualities on the macro-scale.

1.2 OVERVIEW OF TECHNIQUES USED IN ASPHALT MODELLING

The modelling of asphalt behaviour, without particular focus on the compaction process, has been evaluated in a literature research. There are two different approaches used for the numerical modelling of asphalt on the micro-scale: discrete element modelling (DEM) and finite element modelling (FEM). In micro-mechanical research (DEM and FEM) the asphalt material is mostly divided into three different parts: coarse aggregate, mastic and air voids. Coarse aggregates are stone particles larger than a certain size and are often assumed to behave rigid or linearly elastic. The mastic includes the fine aggregates and minor fillers embedded in a matrix of viscous bitumen. The mastic holds the coarse aggregates together and is often considered as a homogeneous material with visco-elastic properties. Since an asphalt mixture contains an enormous amount of mineral particles, which obviously cannot all be explicitly modelled, assumptions about particle sizes in the model are necessary. The air voids percentage is dependent on the asphalt mixture, which can be dense or open, see Figure 2.

In research where the asphalt is considered as a continuum material, the heterogeneity of the mixture is neglected. The material behaviour is then described by a macroscopic material model, often a visco-plastic model.

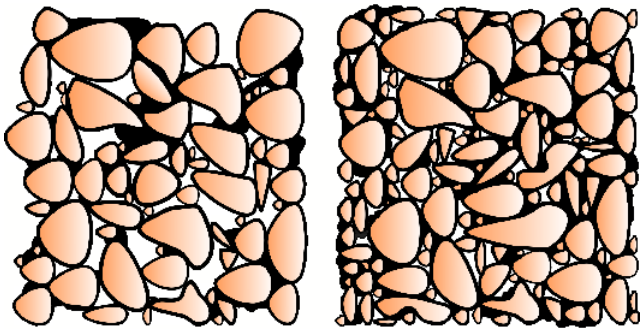

Figure 2: Schematic representations of asphalt material: Aggregate (orange), mastic (black) and air voids (white). The figure on the left represents open asphalt; typically with a high percentage of air void,: the figure on the right represents dense asphalt.

1.2.1 *Modelling Asphalt with DEM*

The discrete element model (DEM) is widely used in engineering problems. It is a numerical technique that solves problems modelled as a system of distinct, interacting, general-shaped (deformable or rigid) bodies or particles subjected to motion and deformation within a certain time span. This time span is divided into multiple steps (time steps). At each time step all forces on the particles or bodies are calculated; integration of Newtons equations of motion gives the translational and rotational behaviour of each body or particle. Because of computational capacity constraints, DEM simulations are limited in time duration and number of particles. In research where DEM is used for modelling asphalt the mixture is often divided into three different phases: coarse aggregate, mastic and air voids [3, 11, 14, 20, 21]. These phases are modelled with spherical or circular particles, depending on the dimension of the model. Most research is performed in two dimensions, although recently three dimensional models appeared [5, 19].

The asphalt aggregate can be considered as a single discrete particle or as a set of particles, in which an irregular aggregate shape can be taken into account. Doing so, a single aggregate is imitated by many (up to thousand) discrete particles, see Figure 3. The same assumptions hold for the mastic. Aggregate parts are assumed to behave rigid or linear elastic; the mastic part behaves mostly visco-elastic.

In more recent research three dimensional particles are used, these particles can be spheres or clumped spheres, creating irregular shapes [5], see Figure 3. Particles can be randomly orientated or placed in a lattice with a certain spacing grid. In a randomly orientated system [5] particles are free to move within the domain; in lattice models [3, 4, 11, 14, 20, 21] particles are clustered together. From literature research it appears that one has tried to use the actual asphalt structure in simulations. By using image technology or CT-scan equipment the surface of a real asphalt sample is imitated and used for particle orientation [2, 3, 14, 20, 21].

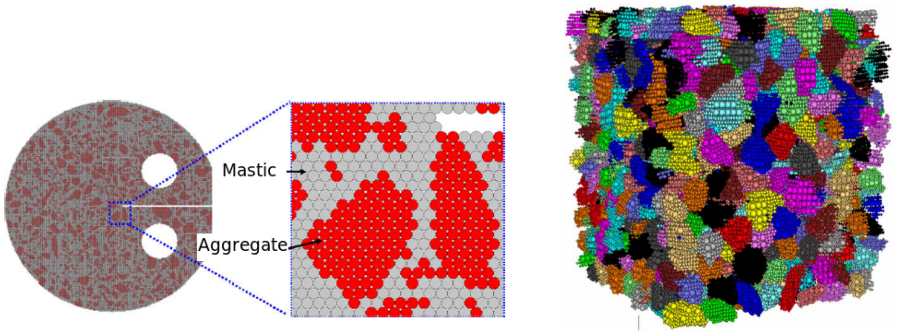

Figure 3: Left: actual asphalt structure imitated with CT-scan equipment and used for the definition of aggregate and mastic, both are built up from multiple discrete particles creating irregular shapes. Right: clumped spheres used to create three dimensional irregular shapes

The most important forces acting during simulation are recoil- (when particles collide), friction- and gravity forces. When an aggregate is built up out of a number of discrete elements, inter-particle cohesion forces are keeping the elements together [20]; the same holds for mastic. A concise overview of different assumptions regarding asphalt modelling with DEM can be found in [21].

Modelling is often carried out with software specifically designed for this purpose (particle flow code, PFC) [4, 5]. DEM modelling of asphalt involves a large number of particles; this limits the usability of the model and makes it incapable modelling entire road behaviour. DEM can be applied to predict the modulus of asphalt samples [21] (often executed with a compression test) as well as for studying fracture behaviour [3].

1.2.2 *Modelling Asphalt with FEM*

The Finite Element Method (FEM) is a numerical technique for finding approximate solutions of a continuous domain, by discretization of the domain into a set of sub domains, usually called elements, see Figure 4. In FEM studies about modelling asphalt on the micro-scale the discretization of aggregate, mastic and air voids is often made. The aggregate and mastic are constructed from different materials [7, 8, 12, 20, 16]. Often FEM is used to model a specific part of the asphalt, for example the mastic behaviour under loading conditions, or the interactions between two aggregates [12]. But FEM simulation can also be used to predict fatigue behaviour like cracking and rutting [20]. A disadvantage is the large amount of computational time needed for modelling asphalt on the micro-scale, since a small volume of asphalt already contains millions of mineral particles. The degrees of freedom required to model each particle are far beyond the currently available computing capacity, even when simplifications are introduced for the definition of aggregate and mastic.

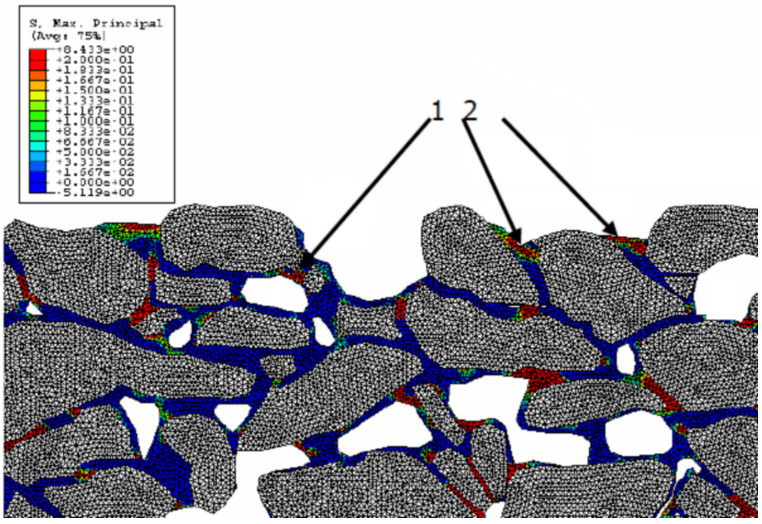

Figure 4: Asphalt structure simulated in FEM; aggregates are defined with white elements and mastic with colored elements.

1.2.3 *Continuum Methods*

In studies where the asphalt mixture is considered as a continuum material the heterogeneity, as well as the micro-scale properties, are neglected. The behaviour is described using a particular material model, often a visco-plastic model, schematically presented by a composition of springs and dampers. These models are used to predict the relation between stresses and deformations in asphalt [6, 13, 15]. Continuum models can also be developed and used in FEM.

1.2.4 *Experimental and Empirical Research on Asphalt*

Empirical research is frequently performed in the professional road branch, but is based on observations and gives no direct insight into the kinematics on the micro-scale, which makes it inefficient for modelling asphalt. Experimental research is usually performed when new asphalt mixtures are developed; these are first tested extensively, before they are used in pavement construction. Experiments are also used for validation of numerical models.

1.2.5 *Summary of Modelling Asphalt*

- Most micro-mechanical models (DEM and FEM) are developed in two dimensions.
- Current DEM models require a large number of particles for the definition of aggregate and mastic.
- Modelling asphalt in detail with FEM requires a large amount of computational time.

- Experimental and empirical modelling contributes little to our understanding of asphalt modelling.
- A Fundamental three dimensional macro-model for compaction is not available.

1.3 RESEARCH DESCRIPTION

Nowadays, compaction is an important topic and a numerical model capable of describing compaction, can contribute to a better understanding of the compaction process, which is useful for constructing better roads. In this research it is tried to construct a model capable of describing asphalt compaction with the use of the DEM model as proposed by Luding [9]. However, this model is not capable of describing the road behaviour (macro-scale); therefore, it is applied on the meso-scale, with micro-scale quantitative parameters. In the second part of this research is investigated how the coupling between meso- and macro-scale can be made. This is achieved by using results from the discrete model in FEM analysis.

A simplified method of compaction is modelled, so called uniaxial compaction, because the realistic modelling of compaction (performed by rollers, or in the laboratory tests), is initially too difficult. For this purpose unique modelling assumptions are formulated to describe the asphalt behaviour during compaction. The model is calibrated by performing laboratory tests of uniaxial compaction; doing so model parameters can be related to the physical properties of asphalt mixtures.

1.4 RESEARCH GOALS

- Investigate if the proposed DEM model is capable of modelling the asphalt behaviour during uniaxial compaction.
- Calibrate the meso-scale DEM model parameters: compare laboratory- with simulation results to relate physical aspects and factors of the asphalt mixture to the model parameters.
- Find out how the micro-based meso-model can be applied to model behaviour on the larger macro-scale.

1.5 OUTLINE OF THESIS

In Chapter 2 the laboratory test of uniaxial compaction of asphalt mixture are explained. In Chapter 3 the theoretical background of the proposed DEM model is explained. Then in Chapter 4 the DEM simulations with the model are clarified, as well as the assumptions required for modelling. The comparison between DEM and experiments is described in Chapter 5. The second part of the research tries to link the the DEM model with a

continuum model, which is described in Chapter 6. Chapter 7 summarizes the performed research, followed by conclusions and recommendations.

2 LABORATORY TESTS

In the laboratory of Reef Infra B.V., a pavement construction company located in Oldenzaal, experimental tests on asphalt mixtures were performed. The intention was to impose a strain-controlled displacement in one direction on the asphalt mixture, which should lead to a compacted sample. These tests should resemble uniaxial compaction, but as far as known, no uniaxial or similar compaction tests have been performed on asphalt mixtures; therefore, successful testing was not guaranteed. In this chapter, first the test setup is described in Section 2.1. The testing of this set up, to find out if it is working properly, is described in Section 2.2. In Section 2.3 is described how asphalt mixtures are uniaxially compacted. In the last Section of this chapter (Section 2.5) physical aspects of the asphalt mixture are related to DEM simulations.

2.1 TEST SETUP

The compaction was performed in a smooth cylindrical mold (inner diameter 112.5 mm, height 150 mm). Mixtures were placed manually in the mold and on top of the mixture a stamp was placed (5277 gr). The weight of the stamp gave some pre-compaction; the stamp moved a little bit downwards when placed on the mixture because of gravity. At this stage, the mixture is ready for compaction: the mold was placed under a press (ASTM D1559 - AASHOT245, see Figure 5) and compaction was started by moving the bottom plate of the press (where the mold is standing on) upwards with a constant velocity $v_{\text{press}} = 0.87$ mm/s. During this movement aggregates are forced together and air is escaping through a narrow space between stamp and mold. The compaction is schematically presented in Figure 5.

The press is linked to a computer program which recorded the displacement of the bottom plate and the corresponding force which the mixture is exerting on the stamp. This data was used for comparison with DEM simulations. The compaction was aborted when the maximum pressing force (50 kn), or the maximum stroke (30 mm), was reached. This press is normally used to determine the strength of compacted asphalt samples in bending tests, but was considered appropriate for our kind of tests, as it was possible to accurately record forces and displacements. However, this testing method has also its limitations: it is unknown whether or not the press rate is appropriate for compaction. Unfortunately, this rate cannot be adjusted. It is also unknown whether the pressing capacity is sufficient or not. Another restriction in this setup is that elastic recovery after compaction cannot be measured.

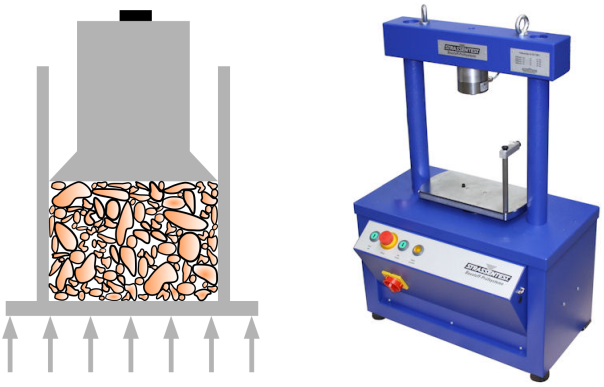

Figure 5: Left: schematic representation of the compaction process, right: the used press for uniaxial compaction.

2.2 COMPACTION TESTS

The described setup was tested by performing trial tests with mixtures of 1 kg aggregate (fraction 8-11.2 mm), together with a quantity of "fake bitumen", also called lubrication oil; see Appendix A for details. After having prepared the mixtures, compaction was started as described in Section 2.1. The results are presented in stress-strain relations in Figure 6; mixture information is given in Table 1. The stress σ is determined by dividing the measured force by the area of the mold and the volumetric strain ϵ_{vol} (for compaction assumed positive) is calculated by dividing the initial sample height by the displacement (measured by the computer linked to the press). The effect of the lubrication oil is clearly visible: the mixture containing 7.5% oil is further and better compacted than the 2.5% oil mixture; higher strain levels are reached and stress levels are lower at equal strain. Note that these tests had actually nothing to do with compaction, as there was no mastic present and many aggregate particles where crushed: see figure 7. Nevertheless, these tests showed that the setup is capable of performing compaction: the pressing force is high enough and detailed stress-strain behaviour can be measured. A restriction of this apparatus is that elastic deformation after compaction cannot be measured, because when the maximum force (or maximum stroke) is reached the bottom plate remains at its attained position and the force drops gradually.

2.3 COMPACTION OF ASPHALT

Two different asphalt mixtures were compacted: (1) an open (or porous) mixture and (2) a dense mixture, both with different kind of bitumen: (1) a hot bitumen, used during pavement construction and (2) a cold bitumen (the "fake" bitumen, see Appendix A), which has similar properties as the hot bitumen at room temperature. The exact composition of these mixtures can be found in Table 1. To imitate the spherical particles as used in the simulations, round aggregate was ordered and used; see Figure 7. Nev-

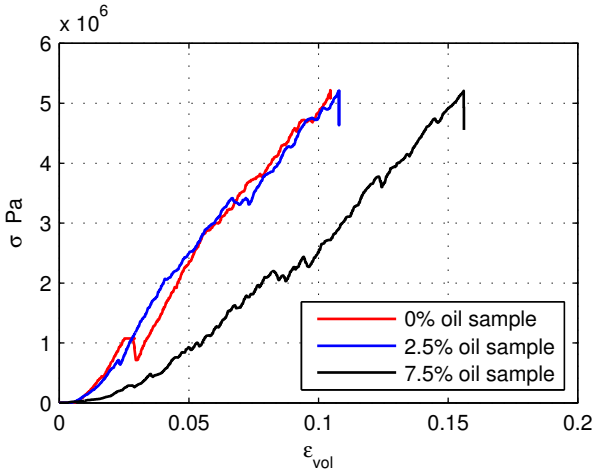

Figure 6: Stress-strain relations during compression of aggregate samples with different percentages of "fake bitumen", see Appendix A, the stress σ is plotted against the volumetric changes ϵ_{vol} (assumed positive during compaction) of the samples. The lubricating effect of the oil is clearly visible, see the 7.5% oil sample; where higher strain levels are reached. These tests are performed at room temperature of approximately 20 °C.

Figure 7: Above: (left) the aggregate sample without oil after compaction; the crushed particles are clearly visible; (right) broken bitumen sample after compaction. The light spots indicate crushed particles. Bottom: (left) the result of compaction with fake bitumen and (right) a cross-section of the asphalt sample with fake bitumen.

Mixture	l_0 mm	ν_0 mm	ν_{final} mm	l_{final} mm	Compaction %
(1) 0 % oil	69.1	0.552	0.616	61.9	10.5
(2) 2.5 % oil	72.2	0.563	0.632	64.4	10.8
(3) 7.5 % oil	77.3	0.588	0.697	65.6	15.6
(4) Open bitumen	63.9	0.623	0.772	54.3	15.0
(5) Open oil	66.7	0.647	0.761	53.7	19.4
(6) Dense bitumen	58.6	0.724	0.848	50.3	14.6
(7) Dense oil	60.6	0.696	0.862	49.0	19.2
(8) Higher sample	122.0	0.695	0.867	97.7	19.9

Table 1: Mixture characteristics before and after compaction

ertheless, these aggregates were still rather angular shaped, hence quite dissimilar to the spherical particles used in the simulations.

The stress-strain behaviour during compaction of the mixtures is given in Figure 8. In all curves two different regions occur: a less stiff region for small strain levels and a stiffer region for higher strain levels. Mixtures with fake bitumen are further compacted and at higher strain levels the stress is lower than in mixtures with hot bitumen. This has two reasons: Firstly: the initial volume fraction ν_0 of the oil samples is lower, resulting in a higher initial sample height l_0; as the oil is more sticky than the bitumen, aggregates are sticking more strongly together, which gives more and bigger air voids. Secondly: the oil is more fluid than the bitumen, which leads to a more fluid mastic and it is to be expected that this will result in better lubrication and compaction.

Although, there is a significant difference in mixture composition, the dense and open mixtures largely show the same stress-strain behaviour. The dense mixtures, with their high percentage of mastic, show a smoother curve, probably because a sudden drop in stress, caused by fraction of a stone, is prevented due to the high amount of mastic. The stress-strain relations are simultaneously displayed on a computer screen and as from stress levels of approximately $\sigma = 2 \cdot 10^5$ Pa the crushing of particles becomes audible.

The open asphalt sample with real bitumen stayed intact after compaction. The obtained density of this sample was measured; it appeared that this density was approaching the desired density obtained with conventional compaction test (Marshall-test). Thus, the performed tests can actually be regarded as compaction. However, it should be noticed that a large number of cracks were present in this and the other samples. Some stones showed little cracks, others were completely crushed; see Figure 7. It can also be seen in this figure that the compaction is not homogeneous; the bottom of the sample looks denser, probably due to the frictional wall effects. 7.

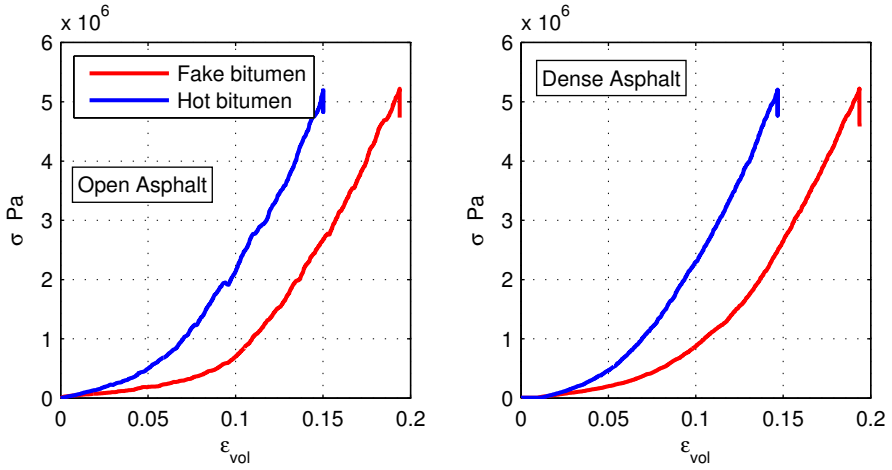

Figure 8: Stress-strain relations during compaction of real open (left) and dense asphalt mixtures, performed in the laboratory of REEF Infra B.V.

Mineral in asphalt mix	Bitumen gr	Oil gr	Density kg/m³
Bitumen 70/100 or SAE	52,13	52,08	1022 or 944
BSH 60 (filler)	43,13	43,09	2493
Coarse sand (filler)	80,76	80,68	2640
Aggregate (< 2,0 mm)	3,22	3,22	2638
Aggregate (2,0 - 5,6 mm)	58,67	58,61	2638
Aggregate (5,6 - 8,0 mm)	167,96	167,80	2638
Aggregate (8,0 - 11,2 mm)	332,13	331,80	2638
Aggregate (11,2 - 16,0 mm)	240,00	239,76	2638
Aggregate (16,0 - 22,4 mm)	21,99	21.98	2638
	Total 1000 gr	Total 999 gr	

Table 2: Minerals of the open asphalt sample and bitumen. 70/100 means the hot-bitumen, SAE means the "fake bitumen", which has similar properties as the hot-bitumen at room temperature.

Mineral in asphalt mix	Bitumen gr	Density kg/m³
Bitumen 70/100 or SAE	85.10	1022 or 944
BSH 40 (filler)	106.3	2700
Coarse sand (filler)	138.4	2640
Aggregate (< 2,0 mm)	24.5	2638
Aggregate (2,0 - 5,6 mm)	346.9	2638
Aggregate (5,6 - 8,0 mm)	467.3	2638
Aggregate (8,0 - 11,2 mm)	66.6	2638
	Total 1000 gr	

Table 3: Minerals of the dense asphalt sample. 70/100 means the hot-bitumen, SAE means the "fake" bitumen.

2.4 ADAPTED SAMPLE HEIGHT

In the performed test a large number of cracks occurred. A lower strain rate may reduce this effect and may lead to better compaction. Unfortunately, it was not possible to adjust the speed of the press. But the influence of strain rate can also be investigated by using a higher (or lower) sample, because the strain rate ($\dot{\epsilon}$) depends on the deformation speed (v_{press}) and the sample height (l_0) as follows:

$$\dot{\epsilon}_{\text{exp}} = \frac{d\epsilon}{dt} = \frac{d}{dt}\left(\frac{l - l_0}{l_0}\right) = \frac{1}{l_0}\frac{dl}{dt} = \frac{v_{\text{press}}}{l_0} \approx \frac{0.87\,\text{mm/s}}{65\,\text{mm}} \approx 0.0134\,\frac{1}{\text{s}} \quad (1)$$

Sample number 8 in Table 1 contains twice as much material as the dense oil-sample, leading to an almost twice as high sample. The compaction of this mixture was aborted, because the maximum stroke (30 mm) was reached. However, stress levels were still lower than the other test. Therefore, the sample was re-compacted in another compaction step. The press was driven back to its original position and the compaction was repeated with the partly compacted sample and continued until the press had reached its maximum pressing capacity. The results of this are given in Figure 9, where stress-strain relations are given of the original and the higher sample. In this figure can be seen that a lower strain-rate (higher sample) has a positive effect on compaction: higher strain levels are reached, and stress levels are lower at equal strain.

2.5 CALCULATION OF DEM MODEL PARAMETERS

During this researched meso-scale DEM model parameters were calibrated by comparing DEM results with experimental results (Chapter 5). Some model parameters are based on the physical aspects of the mixture and are not changed during simulations. This are the following parameters:

- ρ_{solid}, the density of the solid phase. This density equals the density used in the DEM simulations. ρ_{solid} (given in Table 4) is the averaged

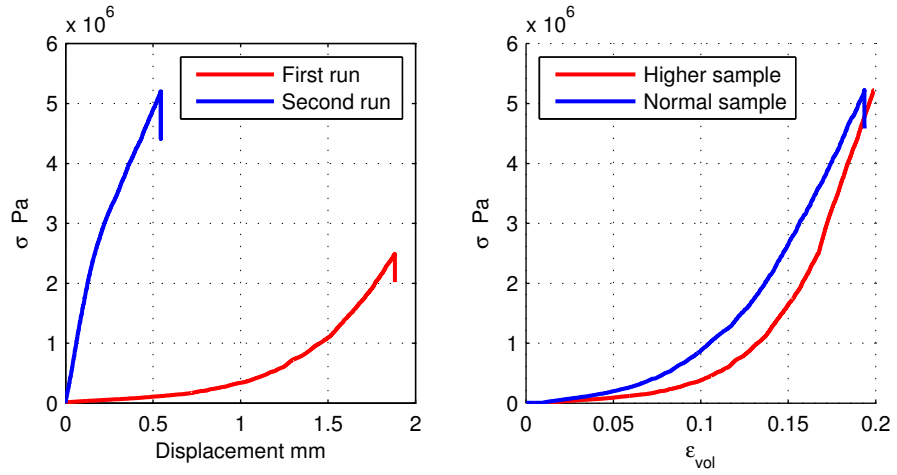

Figure 9: Left: stress-strain relations of the two compaction efforts of the higher sample. Right: stress-strain relations of the higher sample in one curve compared with the normal sample. The effect of an higher sample (which means a lower strain rate) is visible; lower stress levels occur with lower strain rate.

density based on the amount of all solids in the asphalt mixture (aggregate, mineral fillers and bitumen) and can be calculated with the data from Table 2 and 3.

- N, the number of particles in simulations. For simplicity reasons, only aggregate particles larger than 2 mm were taken into account for use in the DEM model. After investigation of the average number of particles present in a certain gradation amount, (this work is not included in this research) it followed that the open asphalt mixture contained 1331 aggregate particles larger than 2 mm.

- ϕ, the plasticity range parameter, defines the amount of mastic in DEM simulation, which in the DEM model is represented by the maximum plastic range $\delta^*_{\max}$ of a particle, see Equation 18 and Figure 12 for better understanding. Assuming two equal particles $a_1 = a_2 = a$ and ignoring for simplicity reasons the pre-factor $\frac{k_2^*}{k_2^* - k_1}$ in Equation 18, Equation 18 then becomes:

$$\delta^*_{\max} = \phi a \tag{2}$$

From this equation follows that the model parameter ϕ, together with the total particle radius a, determines the size of $\delta^*_{\max}$. This parameter is based on V_{m} (the average amount of mastic for one particle), i.e. total amount divided by N) and V_{a} (the average amount of aggregate for one particle), V_{m} and V_{a} can can be calculated using data from Table 2. The sum of V_{m} and V_{a} equals:

$$V_{\mathrm{m}} + V_{\mathrm{a}} = \frac{4}{3}\pi \cdot (a)^3 = \frac{4}{3}\pi \cdot (a_s + \delta^*_{\max})^3 \tag{3}$$

Where $a = a_s + \delta^*_{\max}$. a_s is the inner part of a DEM particle based on V_a:

$$V_a = \frac{4}{3}\pi \left(a_s\right)^3 \tag{4}$$

And $\delta^*_{\max}$ is based on V_m. The plasticity range parameter ϕ can now be calculated using the equations above and is given for the different asphalt mixtures in Table 4.

- p_{ref}, the initial pressure in the asphalt mixture (before compaction) due to the stamp (5 kg) and the mixture (1kg) itself:

$$p_{ref} = \frac{F_{wall}}{A_{wall}} = \frac{\left(m_{stamp} + m_{mixture}\right) \cdot g}{A_{wall}} \approx \frac{6\,\mathrm{kg} \cdot 10\,\frac{\mathrm{m}}{\mathrm{s}^2}}{0.1\,\mathrm{m}^2} = 6 \cdot 10^3\,\mathrm{Pa} \tag{5}$$

Asphalt mixture	ρ_{solid} kg/m^3	plasticity range ϕ
Open bitumen	2432	0.0888
Open oil	2423	0.0898
Dense bitumen	2383	0.1363
Dense oil	2374	0.1376

Table 4: Calculated averaged density of the solid phase (aggregate, fillers and bitumen) for the different asphalt mixtures. And the calculated value for the plasticity range parameter ϕ

2.6 CONCLUSIONS

- The setup is capable of measuring compaction behaviour, the measuring seems adequate, the pressing force is sufficient for particle crushing to occur.
- The tests on asphalt mixtures can indeed be regarded as compaction, as the reached density is in good agreement with conventional compaction tests.
- In all tests particle crushing occurs, at about 2.10^5 Pa.
- A lowered strain rate was leading to better compaction; higher strain levels occurred and the stress levels were lower.
- It was not possible to measure the unloading behaviour after compaction with the used test setup.
- During compaction, there is not much difference in stress-strain relations between the open- and dense asphalt mixtures.
- The tests on the asphalt mixtures were only performed once, reproducibility of the testing has not been investigated.

3

THEORETICAL BACKGROUND DEM

The discrete element model (DEM) is widely used in engineering problems. It is a numerical technique that solves problems modelled as a system of distinct, interacting, and general-shaped (deformable or rigid) bodies or particles subjected to motion and deformation in a certain time span. This time span is divided into multiple steps (time-steps), at each time-step all forces on the particles or bodies are calculated. By integration of Newton's equations of motion the translational and rotational behaviour of each body or particle is described. Too much detail in DEM simulations makes both implementation and interpretation prohibitively difficult. Therefore, in this study a rather simple and objective contact model, presented by Luding [9, 10, 17], is used. This model involves the physical properties of elastic-plastic repulsion, dissipation, adhesion, friction as well as rolling and torsion resistance. In this chapter the theoretical background of the model is explained.

3.1 EQUATIONS OF MOTION

If during a certain time-step all forces acting on particle i, either from other particles, from boundaries or from external forces are known and their sum is $\vec{f}_i$, then motion of particle i is described by integration of Newton's equations of motion. For the translational degrees of freedom this is:

$$m_i \frac{d^2}{dt^2}\vec{r}_i = \vec{f}_i + m_i\vec{g} \tag{6}$$

With m_i the mass of particle i, its position $\vec{r}_i$, the total force acting on the particle $\vec{f}_i$ and the gravitational acceleration $\vec{g}$. For the rotational degrees of freedom:

$$I_i \frac{d}{dt}\vec{\omega}_i = \vec{t}_i \tag{7}$$

With I_i the moment of inertia, the angular velocity $\vec{\omega}_i$ and $\vec{t}_i$ the total torque acting on the particle (due to friction, rolling and torsion). The equations of motion form a coupled system of ordinary differential equations in 2 or 3 dimensions. These equations can easily be solved using an adequate integral solver.

3.2 NORMAL CONTACT FORCE LAWS

The realistic modelling of interacting bodies or particles can be very complicated, for example when occurring deformations and stresses are complicated. Therefore, particle interactions are modelled in a simpler way, by

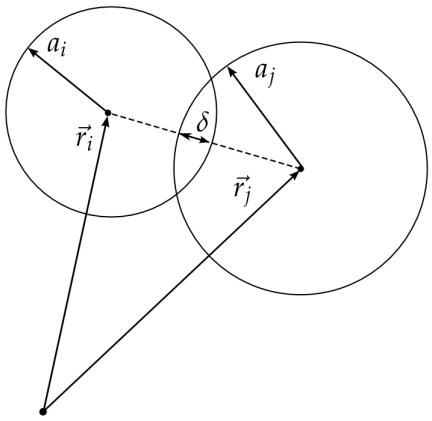

Figure 10: Two spherical particles i and j, with position $\vec{r}_i$ and $\vec{r}_j$ and radii a_i and a_j. These particles interact if their overlap is positive $\delta > 0$.

relating the normal contact force f_n of two particles in contact, with the overlap δ; see Figure 10. The overlap can be defined as:

$$\delta = \left(a_i + a_j\right) - \left(\vec{r}_i - \vec{r}_j\right) \cdot \vec{n} \tag{8}$$

With the unit vector $\vec{n}$ pointing from particle j to particle i, defined as:

$$\vec{n} = \vec{n}_{ij} = \frac{\left(\vec{r}_i - \vec{r}_j\right)}{\left|\vec{r}_i - \vec{r}_j\right|} \tag{9}$$

The force on particle i from particle j at contact c is $\vec{f}^c$, this force can be divided into a normal f^n and a tangential part f^t in the following way:

$$\vec{f}^c = f^n\vec{n} + f^t\vec{t} \tag{10}$$

3.3 NORMAL CONTACT MODEL

The simplest normal contact force model which takes into account excluded volume and dissipation, involves a linear repulsive and a linear dissipative force (in normal direction):

$$f^n = k_n\delta + \gamma_0 v_n \tag{11}$$

Where k_n is the normal stiffness of the two particles, γ_0 is the damping coefficient and v_n is the velocity in normal direction defined as:

$$v_n = -\vec{v}_{ij} \cdot \vec{n} = -\left(\vec{v}_i - \vec{v}_j\right) \cdot \vec{n} = \dot{\delta} \tag{12}$$

With use of Newton's second law we can write f_n as:

$$f_n = -m_{ij}\ddot{\delta} = k_n\delta + \gamma_n\dot{\delta} \tag{13}$$

Where $m_{ij} = m_i m_j / \left(m_i + m_j\right)$ is the reduced mass, rewriting and using the rescaled damping coefficient $\eta_0 = \gamma_0 / \left(2m_{ij}\right)$, the equation for the harmonic oscillator is obtained:

$$\ddot{\delta} + \omega_0^2 \delta + 2\eta_0 \dot{\delta} = 0 \tag{14}$$

This normal contact model is also called the linear spring dash-pot model, it allows to view the particle contact δ as half a period of the damped harmonic oscillator, with initial conditions $\delta\left(0\right) = 0$ and $\dot{\delta}\left(0\right) = v_n$. The contact duration t_c and eigenfrequency ω of the contact are given by:

$$t_c = \frac{\pi}{\omega} \tag{15}$$

$$\omega = \sqrt{\left(k/m_{ij}\right) - \eta_0^2} \tag{16}$$

The contact duration t_c is also of practical importance since the integration of the equations of motion is only accurate if the the integration time-step Δt_{DEM} is much smaller than t_c.

3.4 ADHESIVE ELASTO-PLASTIC CONTACT MODEL

In this research a so called adhesive elasto-plastic contact model is used, a variant of the discussed normal contact model. It reflects permanent plastic deformation, which might take place at the contact and attractive (cohesive) forces can develop for positive overlap. These characteristics are necessary to describe the adhesive particle-particle interaction in the asphalt mixture. In Figure 11, the normal contact force f is plotted against the contact overlap δ. If $\delta < 0$, there is no contact between particles and consequently $f = 0$. The contact force can be written as:

$$f = \begin{cases} k_1\delta \ \left(\text{loading}\right) & \text{if } k_2\left(\delta - \delta_0\right) \geq k_1\delta \\ k_2\left(\delta - \delta_0\right) \ \left(\text{un} - /\text{reloading}\right) & \text{if } k_1\delta > k_2\left(\delta - \delta_0\right) > -k_c\delta \\ -k_c\delta \ \left(\text{unloading}\right) & \text{if } -k_c\delta \geq k_2\left(\delta - \delta_0\right) \end{cases} \tag{17}$$

During initial compressive loading, a contact begins at $\delta = 0$ and the contact force increases linearly with the overlap as $f = k_1\delta$, with k_1 the elasto-plastic contact stiffness. When the compressive loading forces are compensated by the contact repulsive force, the overlap is increased to $\delta = \delta_{\max}$ and the loading is finished. For unloading, the contact stiffness increases to a value k_2, so that the elastic unloading force becomes $f = k_2\left(\delta - \delta_0\right)$, where δ_0 represents the plastic overlap, defined as $\delta_0 = \delta_{\max}\left(k_2 - k_1\right)/k_2$. Reloading at any instant during the unloading leads to an increase of the force along the same line with slope k_2. If the overlap is further decreased ($\delta < \delta_0$), then the contact force becomes attractive (negative). The maximum attractive force $f_{\min} = -k_c\delta_{\min}$ is reached at $\delta = \delta_{\min}$. Further unloading leads to attractive forces on the line $-k_c\delta$ until the contact is broken. The lines with slope k_1 and k_c define the range of possible force values and departure from these lines takes place in the case of unloading and

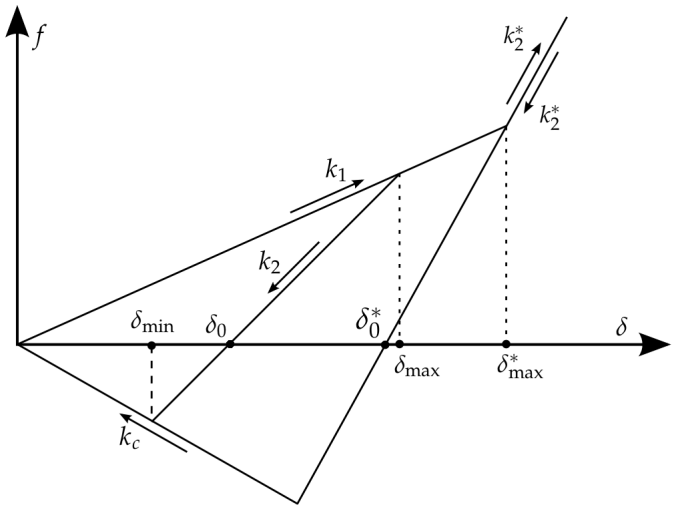

Figure 11: Adhesive force displacement model in normal direction.

reloading. A nonlinear loading behaviour would be more realistic; however, due to a lack of detailed information this piece-wise linear model is used as a compromise. One reasonable refinement, which accounts for an increasing stiffness with deformation, is a k_2 value dependent on δ_{max}. This also implies relatively small and large plastic deformations for weak and strong contact forces. To take this aspect into account an additional model parameter δ_{max}^* is defined:

$$\delta_{max}^* = \frac{k_2^*}{k_2^* - k_1} \phi \frac{2a_1 a_2}{a_1 + a_2} \tag{18}$$

where ϕ is defined as the plasticity depth. If the overlap is larger than δ_{max}^*, the constant stiffness k_2^* is used for loading and unloading. Consequently, also during initial loading the stiffness increases to k_2^* when δ_{max}^* is reached. For $\delta_{max} < \delta_{max}^*$ the stiffness for unloading is interpolated between k_1 and k_2 :

$$k_2(\delta_{max}) = \begin{cases} k_2^* & \text{if } \delta_{max} \geq \delta_{max}^* \\ k_1 + (k_2^* - k_1) \frac{\delta_{max}}{\delta_{max}^*} & \text{if } \delta_{max} < \delta_{max}^* \end{cases} \tag{19}$$

In summary the adhesive, plastic, normal contact model contains 5 parameters k_1, k_2, k_c, ϕ and γ_0 which respectively account for loading, reloading and plastic deformation, adhesion strength, plastic overlap range and viscous dissipation. Note that this model contains the linear normal contact model, because when k_1 equals k_2, then k_c and ϕ become meaningless.

3.5 TANGENTIAL CONTACT

For the tangential degrees of freedom, there are three different force- and torque laws to be implemented: sliding resistance, rolling resistance and torsion, as described in [9]. The unique feature of this tangential contact model is the fact that a single procedure (subroutine) can be used to either

compute, sliding-, rolling- or torsion-resistance. The subroutine needs a velocity as input and returns the respective force or quasi-force. The model parameters for sliding resistance (friction) involve a static and dynamic friction coefficient μ_s and μ_d, a tangential elasticity k_t and a tangential viscous damping coefficient γ_t. For rolling- and torsion-resistance the coefficients μ_r and μ_o are used. Furthermore, there is a rolling and torsion elasticity present k_r and k_o, and viscous damping γ_r and γ_o. A full explanation of the tangential contact model is not given here, but can be found in [9].

4

DEM SIMULATIONS OF COMPACTION

In this Chapter is explained how the DEM model (described in Chapter 3) is used for modelling asphalt compaction. First, in Section 4.1 assumptions are formulated which make the model suitable for describing asphalt behaviour. This involves linking micro-based model parameters with respective physical aspects of the asphalt mixture.

Realistic asphalt compaction, during road pavement or laboratory testing, involves many details which are difficult to model; therefore a simpler method of compaction is presented, so called uniaxial compaction (compaction in only one direction), which can be modelled in DEM.

All DEM simulations in this chapter are carried out in a cubical space confined by walls. The compaction is realised by dictating the motion of the top wall of the cuboidal system (strain-controlled): the top wall moves first downwards till the desired level of compaction is reached and then upwards, back to the original position, which completes the compaction simulation cycle.

During simulation, data about particles in the system, like positions and velocities, energy levels (kinetic- and potential energy), as well as forces acting on the walls, are recorded and written to a file. This data is later used for analysis (see Section 4.3 and Chapter 5). The DEM simulations parameters were calibrated with (actual) uniaxial compaction tests performed in the laboratory, as explained in Chapter 2. In advance of simulating compaction, the uncompacted state of the asphalt has to be created in the DEM environment. This was done in a so called preparation step, as explained in Section 4.2.

4.1 DEM MODEL APPLIED TO ASPHALT MODELLING

The mesoscopic DEM model is built up from spherical particles with different radii. This model has a unique assumption: both mastic and aggregate are modelled in one discrete particle. The inner part of a particle, having radius a_s, represents a stone from the asphalt aggregate and interacts during loading with elastic stiffness k_2, described in the contact model shown in Figure 11. The radius of this inner part is related to the total particle radius a in the following way:

$$a = a_s + \delta^*_{\max} \tag{20}$$

See Figure 12 for a schematic representation and Section 2.5 for further explanation. The mastic represents the outside of every particle (the shell confined by the space between radii a_s to a), and acts with plastic stiffness k_1 during first loading for overlap smaller than $\delta^*_{\max}$. For overlap larger than $\delta^*_{\max}$, the loading/unloading acts with elastic stiffness k^*_2, this represents

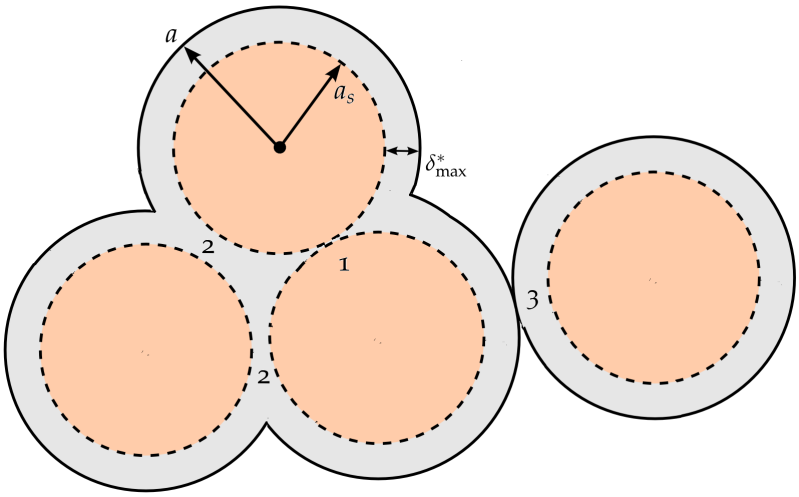

Figure 12: A schematic representation of particles in DEM. The inner parts of particles (physcially representing the stones) are represented by the orange colour and have radius a_s. The mastic layer is represented by the gray layer (the shell as confined by the space between radii a_s to a) and has thickness δ^*_{max}. At point 1 till 4, contacts are present. At contact 1, the mastic layer is squezeed ($\delta \geqq \delta^*_{max}$) and stone-stone interaction takes place. At 2, the overlap is smaller than δ^*_{max} and mastic-mastic interaction takes place. At 3, the contact is beginning and the overlap is small ($\delta > 0$).

Figure 13: This figure shows the cross-section of an open (or porous) asphalt, it is assumed that the modelling assumptions (explained in Section 4.1) compare the best with an open asphalt mixture. These mixtures consists of coarse aggregates and a small amount of mastic.

stone-stone interactions. Summarized: during contact $\delta > 0$: first mastic-mastic interaction takes place and for deformation $\delta > \delta^*_{max}$ stone-stone interaction occurs.

In practice these model assumptions correspond best with an open asphalt mixture, which consists of coarse aggregates and a small amount of mastic, see Figure 13. For this reason, it is decided to simulate and experiment with open asphalt. Stone particles larger than 2 mm in the asphalt mixture are regarded as particles in DEM, which results in 1331 particles (for further explanation see Section 2.5). A value of $\phi = 0.1$ is chosen, see Section 2.5. This value differs slightly from the calculated value, but is for simplicity chosen to be 0.1 in all simulations. The density in the simulations is chosen to be $\rho = 2000\,\mathrm{kg/m^3}$. This does not exactly conform with ρ_{solid} calculated in Section 2.5. In the first performed simulations $\rho = 2000\,\mathrm{kg/m^3}$ was taken as first guess, since this density does not differ a lot from ρ_{solid}

and already many simulations were performed with $\rho = 2000\,\mathrm{kg/m^3}$, the density value was not changed.

The first simulations results already were in good qualitative agreement with the experimental tests. When scaling up the simulations with a constant factor by adjusting the unit of time, which is allowed, see Section 5.2. This suggests that it is not necessary to search for realistic values for k_2, but one has to consider the unit of time. Note that all simulations in this research (except the scaling test in Section 5.2) were performed with the so called non-dimensional units (third column of Table 6) and that the simulation results were scaled afterwards with the adapted unit of time t_u, which makes the results dimensional. For a detailed explanation of this scaling procedure, see Sections 5.1 and 5.2.

Due to the presence of k_t, particles stick to each other. From first simulations it followed that k_t has negligible influence in compaction simulations; however, k_t may influence the preparation, but this has not been investigated in this study. Temperature dependency, which affects the behaviour of the bitumen (μ, k_1, k_t or γ_n) , is also not taken into account. In order to study the effect of friction, various friction coefficients $\mu = \mu_s = \mu_d$ were used in simulations.

The model contains viscous, i.e. velocity rate dependent damping in the form of a normal viscosity γ_n, tangential viscosity γ_t and background viscosity γ_b. The normal- and tangential viscosity have not been varied in the simulations, since these will be strongly temperature dependent and no knowledge about this dependency is available. The background damping is continuously acting on the particles; this can be regarded as the resistance to particle motion due to an excess of mastic, since in practice not all the mastic will be equally spread out around the particles. This parameter has also been chosen constant.

Gravity has been omitted from the model, because it might affect the preparation step by creating an isotropic sample and during compaction the influence of gravity is negligible, as the reached compression pressure is many orders of magnitude higher.

These modelling assumptions result in a very simple model: a system consisting of 1331 spherical particles only, which represents a small volume (cuboid) of asphalt. Moreover, exact geometrical properties and realistic stress distributions are ignored, as spherical particles are used and interaction forces are related to the overlap. It is assumed that the mastic behaviour can be described with model parameters: k_1 (the plastic stiffness) and μ (the friction coefficient), the amount of mastic with ϕ and stone behaviour with k_2. These meso-scale model parameters will be calibrated by experimental tests and if successful, further analysis, or other parameters on the micro-scale will become redundant. To summarize, the most important assumptions explained in this section are:

- Aggregate and mastic are in DEM modelled as one spherical particle; the inner part represents the stone and the outer shell the mastic. Both parts acts with different stiffness during loading/unloading.

- Mineral particles larger than 2 mm in asphalt mixtures are regarded as aggregates; smaller particles are regarded as part of the mastic. With these assumptions only 1331 particles are necessary in DEM for the representation of an open asphalt mixture with a volume of 0.001 m^3.
- Exact geometrical properties and realistic stress distributions are ignored.
- By calibrating the model, it is tried to relate meso-scale model parameters to physical aspects of the asphalt mixtures.

4.2 SAMPLE PREPARATION

During preparation the non-compacted state of asphalt is created, which is the starting point of the compaction process, as described in Section 4.3. During the switch between the preparation and compaction simulation, it is not allowed to change stiffness parameters, because these determine the contacts between particles. It appeared that the preparation step was an important step, which even can dictate the outcome of the compaction simulation. This is undesirable, since the primary goal is modelling compaction independent of preparation.

It appeared that the loading stiffness k_1, friction coefficient μ and volume fraction v (of the non-compacted state) have significant influence on the non-compacted state, which then possibly can affect compaction. It would be conform reality if this state is always the same, but unfortunately this is not the case. This signifies the need of a well controlled procedure for preparation (before compaction starts), in both simulations and experiments.

Preparation as well as compaction take place in a cuboidal volume with initial volume $V_0 = L_0^3$ confined by walls, with $L_0 = 0.1$ m. The preparation simulation starts by reading initial data from a file, such as particle positions, radii and random velocities. Simultaneously, properties like density, stiffness and friction are assigned to the particles. This gives the user a lot of freedom in creating a structure; however, the preparation must be easy, reproducible and as much as possible true to reality (the experiments from Chapter 2).

Because of the made assumptions regarding the mastic and aggregate, realistic geometry is neglected; therefore, no effort is put in creating a cylindrical asphalt structure as used in the experiments. However, for consequent and reproducible modelling it is required that the non-compacted initial state is solid and isotropic. Solid means that the system is at rest (no moving particles) and particles are overlapping each other, the latter implies low kinetic- to potential-energy ratio and a coordination number C larger than 3. The kinetic energy is present in the movement of the particles and the potential energy in the overlap between particles. The coordination number is defined as:

$$C = \frac{M}{N} \tag{21}$$

Here M is the total number of contacts and N is the total number of particles. It is chosen to make the non-compacted state isotropic, as it is assumed that this is more or less the case in the experiments. All preparation steps start with reading in the same initial particle data and have properties defined in Table 6. During this researched three methods are investigated for creating an easy, reproducible, solid and isotropic initial state. The 3 methods are shortly described below and will be detailedly explained in the following Sections (4.2.1, 4.2.2 and 4.2.3).

- Swelling 1: particles are growing in size until a target volume fraction of $v = 0.5$ is reached. This method leads to isotropic particle systems with unequal strength, moreover particle systems with high k_1 did not form a solid material yet, which affects the behaviour during compaction.
- Swelling 2: particles are growing in size until a target pressure level is reached on the walls of the cuboidal volume. This methods leads to isotropic particle systems of equal strength and show the same behaviour at the start of compaction. However, the volume fraction after the reached target pressure differs for variable k_1; this might seem not to be realistic.
- Pressure control: particles are growing in size until a target volume fraction of $v = 0.425$ is reached; next, a target wall pressure is obtained, by moving the walls of the cuboidal volume inwards. This method leads to isotropic particle systems of equal strength and show the same behaviour at the start of compaction. The swelling until a target volume fraction of $v = 0.425$ is necessary to create an isotropic system, but this is also leading to some initial strength, which affects the reaching of the target pressure on the walls.

4.2.1 *Swelling 1*

The first effort to create an initial state is performed by a process called swelling 1. During this process particles are growing in size until a desired volume fraction is reached. The process starts with 1331 particles having initial radii a_0 (uniformly distributed between 0.001 m and 0.0045 m), these are placed on a square lattice in V, resulting in an initial volume fraction $v_0 = 0.1611$.

The system is then allowed to evolve to a disordered state, by attributing random velocities (magnitude and direction) to the particles. For this randomization it is very important that the initial volume fraction is very low, otherwise the system has no chance to become random and could depend on the initial (user-defined) structure. Simultaneously the particle radii are exponentially increasing:

$$a(t) = a_0 e^{g_r t} \tag{22}$$

Where t is the simulation time and g_r the growth rate factor. This leads to the volume fraction as function of time:

$$v(t) = v_0 e^{3 g_r t} \tag{23}$$

The growth is stopped when the target volume fraction v_{max}, is reached, or when the simulation time has passed. When v_{max} is reached, the system is relaxed: the particle growing is stopped and in the remaining simulation time the system is becomes static: the kinetic energy (E_{kin}) is tending towards zero and the external hydrostatic pressure (p_0) is becoming constant. A solid state is reached at v_{max} when $E_{kin}/E_{pot} \ll 1$ and $C > 3$ (the coordination number, defined in Equation 21). C must be larger than 3 in order to represent a solid material with friction present.

In this first effort swelling takes place with variable friction $\mu = 0.1 - 0.4$ and plastic stiffness $k_1 = 10 \cdot 10^5 - 40 \cdot 10^5 \,\mathrm{N/m}$, constant elastic stiffness $k_2 = 100 \cdot 10^5 \,\mathrm{N/m}$, growth rate $g_r = 0.1 \cdot \frac{1}{\sqrt{\frac{1}{10^5}}} \frac{1}{s}$, and simulation time $t = 8 \cdot \sqrt{\frac{1}{10^5}}$ s, until a volume fraction of $v_{max} = 0.5$ is reached. v_{max} is chosen lower than the volume fraction of non-compacted asphalt in the laboratory tests, because the void space is expected to be larger when spherical particles are used instead of angular particles, as in the laboratory tests. This choice is not further studied but just taken as first guess.

The results of this preparation method (swelling 1) are depicted in Figure 14 for variable k_1 and constant μ. This figure shows: the energy ratio, defined as the kinetic- divided by the potential energy (left top), the coordination number (right top), the hydrostatic pressure (left bottom) and the volume fraction (right bottom). From the energy ratio plot, the coordination number plot and the pressure plot, one can see that particle systems with higher plastic stiffness $\left(k_1 \gtrapprox 30 \cdot 10^5 \,\mathrm{N/m}\right)$ were not forming a solid material. These systems can be regarded as loose or even fluid, which will result in weaker behaviour during compaction, especially at the start, when compaction makes the particle systems solid. The fact that particle systems with lower stiffness are not forming a solid is not fully understood, probably particles act softer, meaning that less force is needed for (plastic) deformation and contacts. The exact reason for this phenomena is not investigated in this research. Nevertheless, this behaviour is undesirable, since the k_1 parameter cannot be chosen freely.

In summary the swelling 1 method is most easy to implement. It requires the arbitrary choice of v_{max} or k_1, such that a well defined end-state can be reached. However, these states have an unpredictable strength, which is a strong disadvantage.

4.2.2 *Swelling 2*

In the second preparation method it is tried to create equally strong samples during preparation. The preparation is again performed with swelling (explained in the Section 4.2.1), but now v_{max} is made variable: swelling is performed until a volume fraction range of $v_{max} = 0.4 - 0.55$. Then the

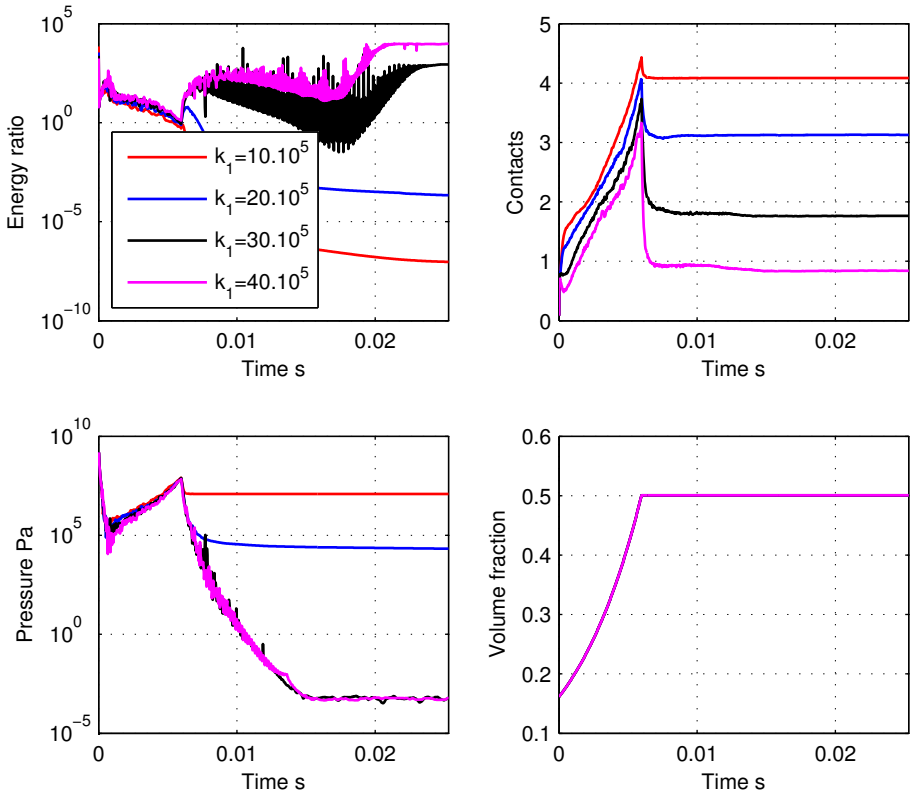

Figure 14: Plots of particle system characteristics during preparation method Swelling 1 $k_2 = 100 \cdot 10^5\,\mathrm{N/m}$, $\mu = 0.1$, the range of values for k_1 is given in the legend. Swelling occurs until volume fraction $v_{\max} = 0.5$ is reached, hereafter particle systems are relaxing. Particle systems with high plastic stiffness ($k_1 \geq 30 \cdot 10^5\,\mathrm{N/m}$) are not solid after relaxation, because the energy ratio (top left plot) is too high and the coordination number C (top right plot) too low

hydrostatic pressure, that is the average pressure particles are exerting on the walls (after relaxation), is determined and compared with the assumed starting pressure in the experiments p_{ref}; see Section 2.5. Sample prepared in this way should, for variable k_1 and μ, each display the same p_0; only the corresponding volume fraction varies.

This preparation was leading to an interesting phenomenon: particle systems with lower friction have a higher volume fraction at p_0; see Figure 15. Probably, with lower friction present, it is easier for particles to occupy void space and as result less pressure is built up. This effect is dominant in compaction; denser samples are simply much harder to compact; see Figure 21; where can be seen that samples with lower friction are showing stiffer behaviour during compaction. This phenomenon is unwanted, as it is tried to relate the friction coefficient to bitumen properties during compaction. For this reason, it was decided to skip the friction dependency in the preparation step and to use a constant friction coefficient of $\mu = 0.2$ instead.

This method of preparation is not practical, because a whole range of analyses have to be performed to find the correct target pressure and there is still some variation in p_0 after relaxation (see Figure 16 the left bottom plot), which can be contributed to the coarse volume fraction range and to the growth rate. With a finer volume fraction distribution and a smaller growth rate this may be reduced.

In summary, the swelling 2 method is leading to an isotropic, solid state and an almost equal initial pressure p_0, while the volume fraction is variable. However, this method is not practical; since the target p_0 was searched by performing multiple analyses with variable volume fraction. It followed that the reached volume fraction at the target pressure is depending on μ, which is unwanted, since it affects the compaction results. For this reason constant μ is chosen in simulations.

4.2.3 *Pressure Control*

To enhance and reduce the steps in the previous preparation swelling 2 (see Section 4.2.2), a new preparation method, called pressure control, was developed. This method actually consists of 2 different steps: first the system is swelled (following the same procedure as described in Chapter 4.2.1) until an artificially low volume fraction $\nu_{\text{max}} = 0.425$ is reached, after which it is relaxed. At this stage it is assumed that particle systems are not yet a solid material.

Next, the particle systems are pressurized in all directions by moving the walls of the cuboidal system in a pressure controlled mode inwards, until a certain reference pressure p_{ref} on the walls is reached. This pressure results from the forces of particles that are in contact with the wall. Walls can move outwards when the current pressures is higher than p_{ref}. The magnitude of p_{ref} is set identical to the initial pressure that is present in the compaction experiments due to the present of the stamp; see Section 2.5. When p_{ref} is reached, the wall motion is stopped.

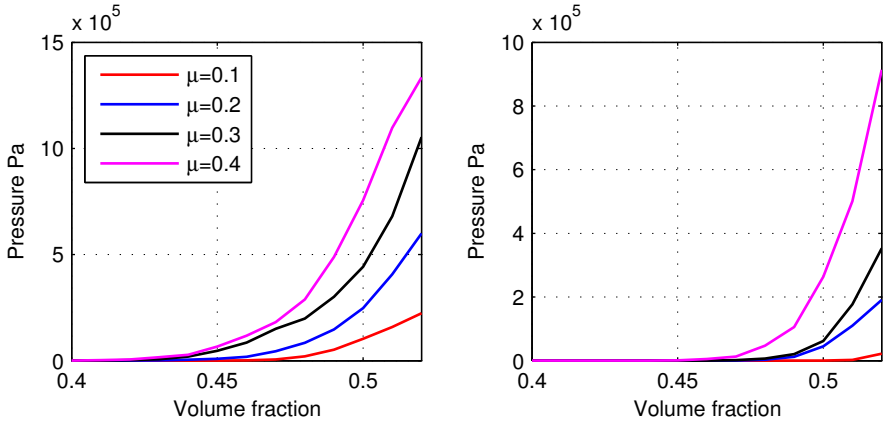

Figure 15: Particle systems prepared with the Swelling 2 method. These plots give the hydrostatic pressure (averaged over the 6 walls of the cuboidal volume) after relaxation as function of the volume fraction; left $k_1 = 10 \cdot 10^5\,\mathrm{N/m}$, right $k_1 = 20 \cdot 10^5\,\mathrm{N/m}$. Systems with lower friction have a higher volume fraction at the the target pressure, which is leading to stiffer behaviour during compaction, see Figure 21. This phenomena is unwanted and therefore friction is skipped during preparation.

A slight adaptation in parameters was necessary for this preparation, because the relative high background damping was leading to a too long relaxation time (see the agreement with an over-damped system), which was leading to a continuous increase in volume fraction. The results of this preparation are presented in Figure 17. This method is actually somewhat better than the swelling 2 method: there is less kinetic energy present, resulting in a lower energy ratio and thus a "more solid" material is created.

In summary: the pressure control mode is easy to implement and leads to solid initial state. However, this method has the disadvantage that the necessary swelling affects the pressure control mode: some initial strength was present which affects the control mode; see Figure 18, where the system with $k_1 = 10 \cdot 10^5\,\mathrm{N/m}$ shows characteristics of a solid material at volume fraction $v = 0.425$. This can clearly be seen in the pressure control mode; see Figure 17 (plot bottom right), where the system with lowest $k_1 = 10 \cdot 10^5\,\mathrm{N/m}$ has a significant lower final volume fraction: there is initial strength as a a result of swelling, which causes the walls to move less far inwards.

To compensate for this effect, swelling until an even lower volume fraction $v = 0.3$ was performed. Particle systems were definitely not solid at this volume fraction, but the isotropic structure was not guaranteed when using the pressure control method, because visual inspection learned that particles were sticking to the moving walls during the pressure control mode. However, no detailed investigation on this phenomenon was performed.

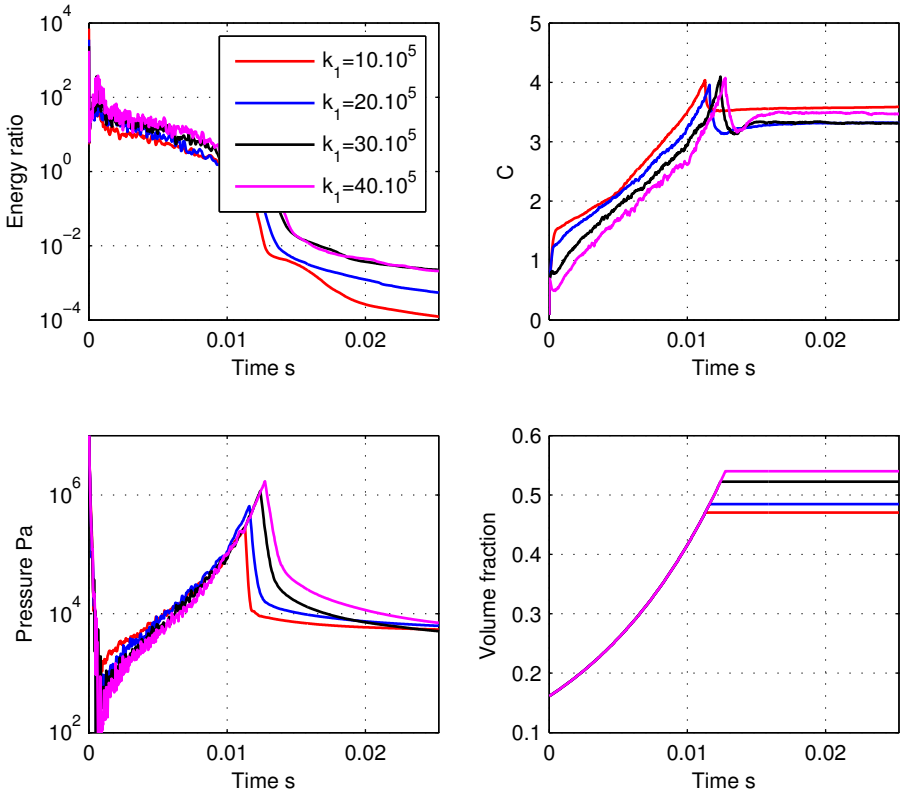

Figure 16: Plots of particle system characteristics during preparation method Swelling 2; $k_2 = 100 \cdot 10^5\,\mathrm{N/m}$, $\mu = 0.1$. Swelling is performed until a volume fraction range of $v_{\max} = 0.4 - 0.55$. Then, the hydrostatic pressure, that is the average pressure particles are exerting on the walls (after relaxation) is determined and compared with $p_{\mathrm{ref}} = 10^3$ Pa; see Section 2.5. The particle systems which show the best agreement with p_{ref} (for variable k_1) are plotted in the figures. In this way of preparation the volume fraction (bottom right plot) is variable. .

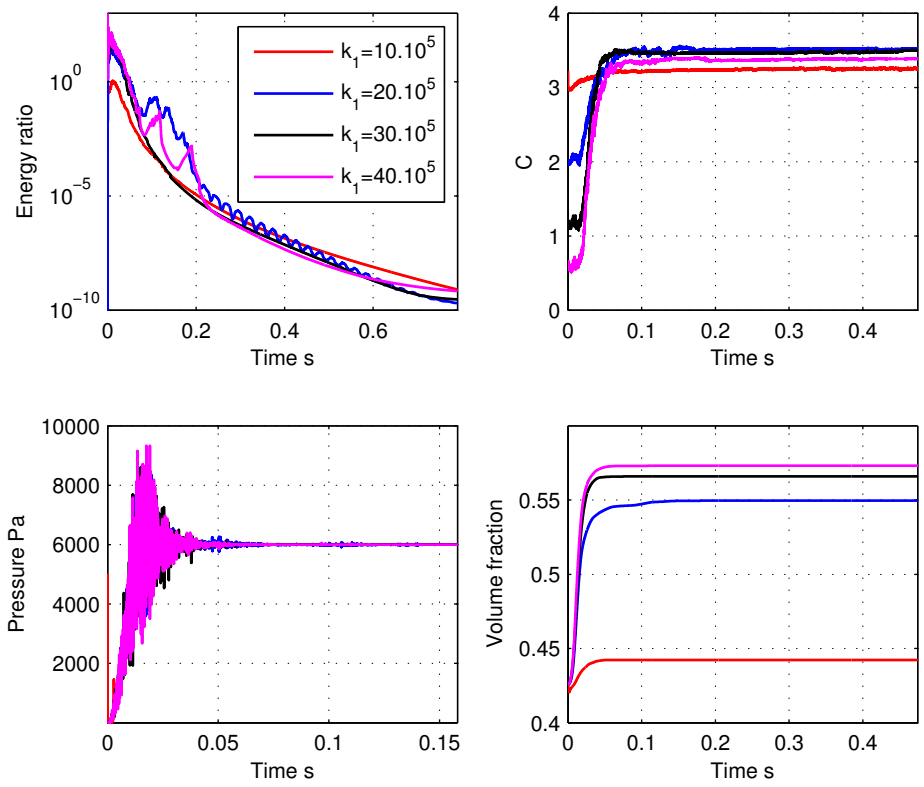

Figure 17: System behaviour under pressure control preparation mode with variable k_1 $\mathrm{N/m}$ as given in the legend and $\mu = 0.2$. First, the systems are swelled as described in Section 4.2.1 until a volume fraction $v = 0.425$ (not shown in these plots). Then, during pressure control (the displayed plots), the walls of the cuboidal system are moving inwards until the target pressure is reached (bottom left plot). The difference in reached volume fractions is clearly visible (plot right under): the system with $k_1 = 10 \cdot 10^5$ $\mathrm{N/m}$ differs significantly from the other ones, probably due to the presence of initial strength caused by swelling.

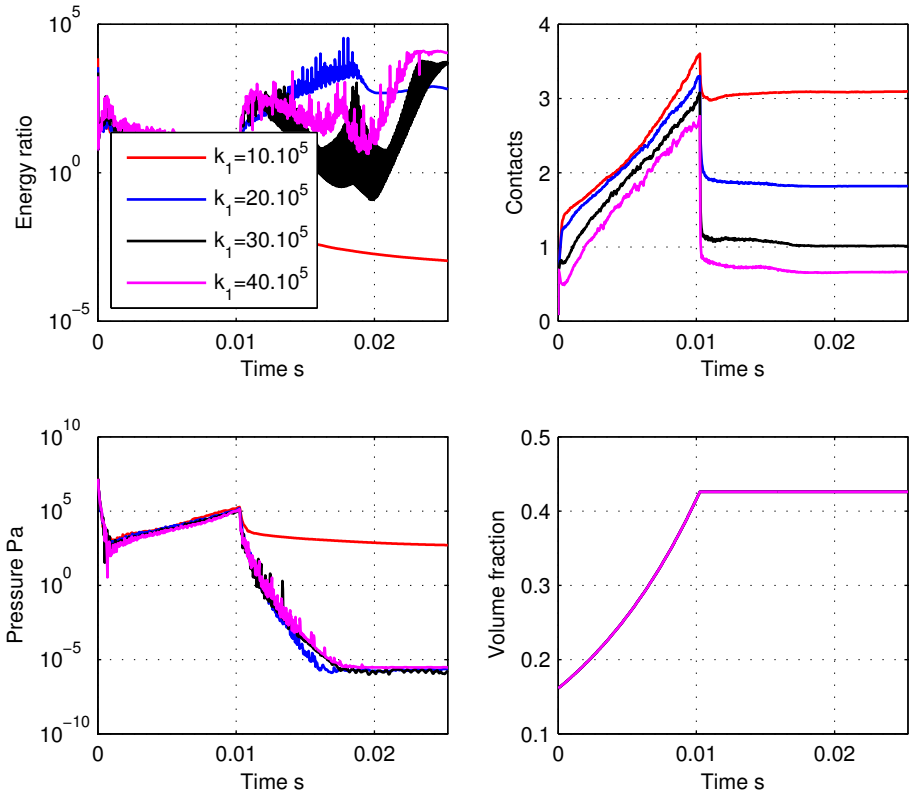

Figure 18: Plots of particle system characteristics during swelling until volume fraction $v = 0.425$. Energy ratio plot (top left) and contact number plot (top right). $k_2 = 100 \cdot 10^5\,\mathrm{N/m}$, $\mu = 0.1$, while the range of values for k_1 is given in the legend. The particle system with plastic stiffness ($k_1 = 10 \cdot 10^5\,\mathrm{N/m}$) was already forming a solid material after relaxation.

4.2.4 *Conclusions Sample Preparation Procedures*

- Choosing a fixed target volume fraction during preparation method Swelling 1 (Section 4.2.1) is not recommended, as this causes a huge difference in sample strength for different stiffness parameters, which affects the compaction results.
- Equally strong isotropic samples were created in Section 4.3.2 and 4.3.3. This gives equal starting points in the stress-strain curves during compaction. Although the volume fraction differs, which is not realistic, this preparation is recommended.
- Variable friction in preparation is undesirable, as particle systems with lower friction are denser at the target pressure (preparation swelling 2 Section 4.2.2). This will influence the compaction, see Figure 21, which is unwanted, as it is tried to relate μ to mastic properties.
- The pressure control method is leading to "more solid" samples: the kinetic energy is reaching zero and the pressure is becoming constant. But this method needs some inital swelling in advance, otherwise the isotropic structure is not guaranteed, because particles will stick to the wall during motion. It should be noted that this pre-swelling, especially for a very low k_1, can lead to some initial strength, which causes the pressure control to stop earlier, see the $k_1 = 10 \cdot 10^5\,\mathrm{N/m}$ sample in Figure 17 (bottom right plot).
- The swelling 2 method (Section 4.2.2) avoids the problem stated in the point above, but extra effort is needed to find the correct volume fraction for the desired initial pressure. Therefore, a range of volume fractions must be investigated and the system with the correct strength (pressure) must be chosen. This method can be improved by chosing a lower growth rate, in which case the final pressure in Figure 16 (left bottom plot) will differ even less. This preparation step and corresponding compaction was chosen for further analysis with the experiments in Chapter. 5.

4.3 COMPACTION

Compaction is always done with a relaxed end configuration after preparation. The compaction is realised by moving the top wall of the cuboidal system downwards until a volumetric strain $\epsilon_{\mathrm{vol}} = -\frac{\Delta L}{L_{\mathrm{tot}}} = 0.2$ (defined positive for convenience) is reached, where ΔL is the inward displacement of the top plate and L_{tot} is the initial sample- or system height. In the case of pressure control preparation, the maximum volumetric strain is slightly higher, because the volume is already reduced during preparation. The downwards movement takes place with a sinusoidal velocity profile with period $T_{\mathrm{compaction}} = 10 \cdot \sqrt{\frac{1}{10^5}}$ s (thus $^{\mathrm{T}_{\mathrm{compaction}}}/_2$ s loading and $^{T_{\mathrm{compaction}}}/_2$ s

Preparation:	$k_1 = 10 \cdot 10^5$ N/m	$k_1 = 20 \cdot 10^5$ N/m	$k_1 = 30 \cdot 10^5$ N/m	$k_1 = 40 \cdot 10^5$ N/m
Swelling 1	$v_0 = 0.500$	$v_0 = 0.500$,	$v_0 = 0.500$	$v_0 = 0.500$
Swelling 2	$v_0 = 0.446$	$v_0 = 0.485$,	$v_0 = 0.522$	$v_0 = 0.540$
Pressure control	$v_0 = 0.442$	$v_0 = 0.550$	$v_0 = 0.566$	$v_0 = 0.573$
Swelling 1	$p_0 = 2.96 \cdot 10^5$	$p_0 = 4.42 \cdot 10^4$	$p_0 = 2.37 \cdot 10^{-6}$	$p_0 = 3.73 \cdot 10^{-6}$
Swelling 2	$p_0 = 5.43 \cdot 10^3$	$p_0 = 6.26 \cdot 10^3$	$p_0 = 5.08 \cdot 10^3$	$p_0 = 7.03 \cdot 10^3$
Pressure control	$p_0 = 6.00 \cdot 10^3$	$p_0 = 6.00 \cdot 10^3$	$p_0 = 6.00 \cdot 10^3$	$p_0 = 6.00 \cdot 10^3$

Table 5: Volume fractions (v_0) and averaged hydrostatic pressure (p_0 in Pa) after different preparation methods with variable k_1 (see the table), $k_2 = 100 \cdot 10^5$ N/m and $\mu = 0.2$.

unloading (note that here the unit of time is scaled, in order to create realistic, dimensional units, see Section 5.2) and amplitude $a_{\text{compaction}} = 0.02\,\text{m}$. The results of compaction are presented in stress-strain relations, by plotting the strain (ϵ_{vol}) versus the stress on the bottom wall $\sigma_{\text{wall}} = \frac{F}{A}\,\text{N/m}^2$, where F is the force on the bottom wall with area A. The stress distribution on the bottom wall is chosen, as this is conform to the experiments.

All particle systems created in the previous chapter are compacted, their starting volume fraction and hydrostatic pressure are summarized in table 5. The following compaction simulations are presented and discussed:

- Compaction Preparation Swelling 1 (Section 4.3.1), particle systems were created as described in Section 4.2.1.
- Compaction Preparation Swelling 2 (Section 4.3.2), particle systems were created as described in Section 4.2.2.
- Compaction Pressure control 1 (Section 4.3.3), particle systems were created as described in Section 4.2.3.

4.3.1 *Compaction Preparation Swelling 1*

The compression stress-strain relations are given in Figure 19, where the stress on the bottom wall σ versus volumetric strain ϵ_{vol} (assumed positive) for variable k_1 and μ are plotted. Approximately, two different regions can be seen in these plots: (1) a low stiffness region for $\epsilon_{\text{vol}} < 0.1$ and (2) a much stiffer region for higher strain levels. The "not solid" non-compacted state of the particle systems with $k_1 = 30 \cdot 10^5$ N/m; $40 \cdot 10^5$ N/m can be seen in the the stress-strain curves, where initially extremely soft behaviour for small ϵ_{vol} occurs and later, when the system is becoming solid, the final maximal stress rises above curves with lower k_1. This is to be expected, as higher stiffness should always lead to higher stresses in this strain controlled compaction method.

Also the starting stress (at zero strain) differs significantly for different values of k_1, as a result of the swelling process. Higher friction is leading to higher stresses which seems logical: higher friction gives the particles more

resistance in reaching empty void spaces during compaction, resulting in less contacts, but higher overlap and potential energy. Finally, during unloading (the upwards movement of the wall) more elastic recovery (due to the higher potential energy) is present for larger coefficients of friction, resulting in less compaction, as illustrated in Figure 20.

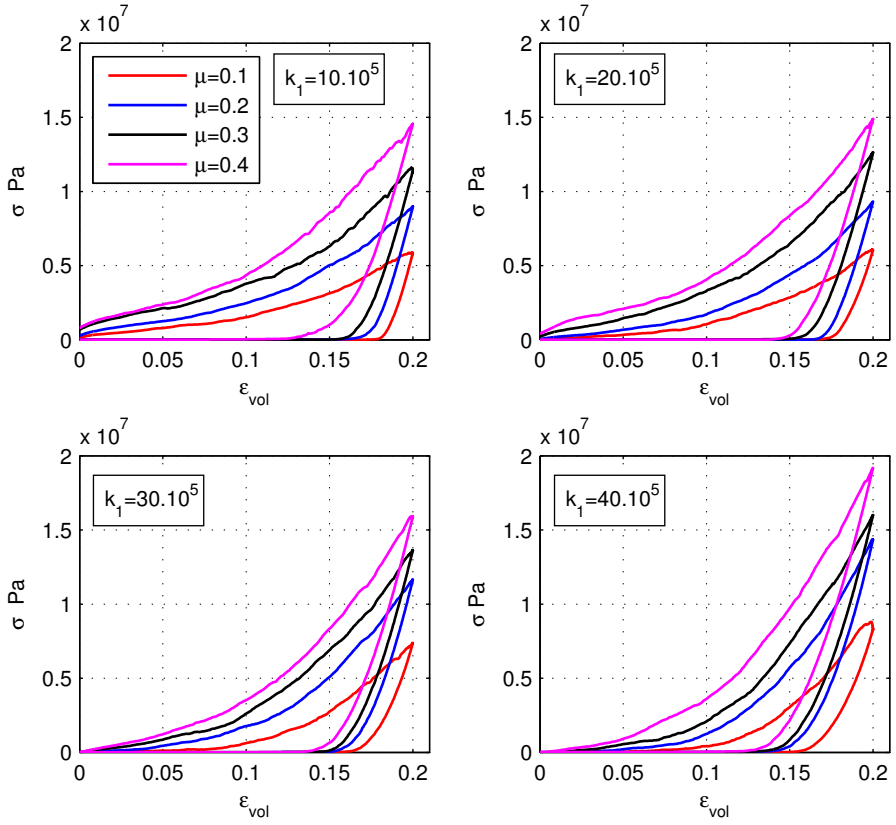

Figure 19: Stress-strain relations during compaction for different μ and $k_1$in $^{N}/_{m}$ (see the legend and boxes). Due to the preparation, the samples are not equally strong (see the differences in p_0 in Table 5); systems with higher k_1 show initially softer behaviour, because they are not solid yet.

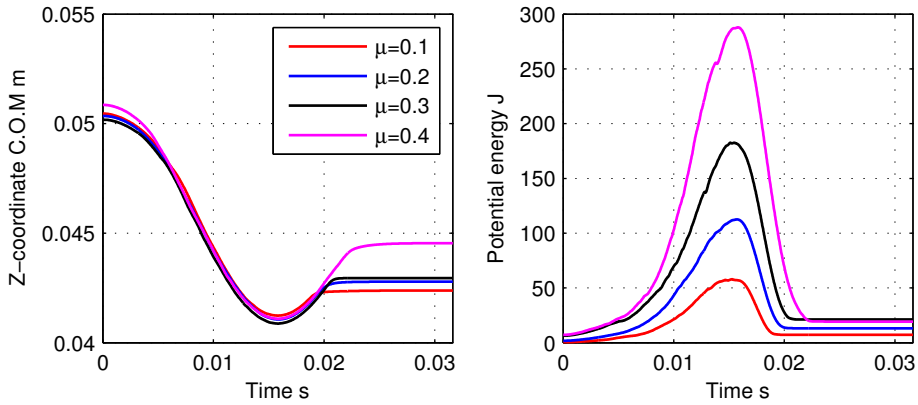

Figure 20: Higher friction is leading to more potential energy during compaction (right plot), which results in more elastic recovery (during unloading) and less compaction; see the left plot, which shows the Z-position (compaction direction) of the center of mass. $k_1 = 10 \cdot 10^5$ N/m.

4.3.2 *Compaction Preparation Swelling 2*

The stress-strain relations during compaction of samples prepared with swelling method 2 (Section 4.2.2), are presented in Figure 21 and 22. Figure 21 shows the difference between constant and variable friction in preparation. As explained, lower friction was leading to denser samples in preparation, what is also clearly visible in the left plot in Figure 21, where the system with the lowest friction coefficient $\mu = 0.1$ is showing the stiffest behaviour. This of course is counter-intuitive; the friction force increases with μ and should offer more resistance during compaction. Therefore, it was decided to skip the friction dependency in preparation and use a constant friction coefficient of $\mu = 0.2$ instead.

The stress-strain relations during compaction with constant friction $\mu = 0.2$ during preparation are shown in Figure 22. It is remarkable that the shape of the stress-strain curves changes with increasing k_1. When k_1 increases, the shape of the curve becomes almost linear. This can be explained as follows: the samples with lower stiffness, have a significant lower starting volume fraction, see Table 5. As a consequence, more and larger void spaces, where particles can intrude during compaction are present, so that they don't have to interact immediately. This is in contrast with the higher stiffness (the starting volume fraction is higher after preparation), where the particles interact earlier and more potential energy is built up. This is illustrated in Figure 23; the sample with higher stiffness has a higher coordination number and more potential energy is built up.

During unloading this potential energy will be released, with k_2^* or k_2 (the maximum stiffness during stone-stone) interactions. The denser samples contain much more potential energy and are showing much more elastic recovery, see the Z-coordinate C.O.M. plot (right bottom in Figure 23). This plot shows the average Z-coordinate of the center of mass, which is initially 0.05 and reduced to about 0.042, in case of perfect compaction this

should be 0.04. Accordingly the top half of the system is more compacted than the bottom half.

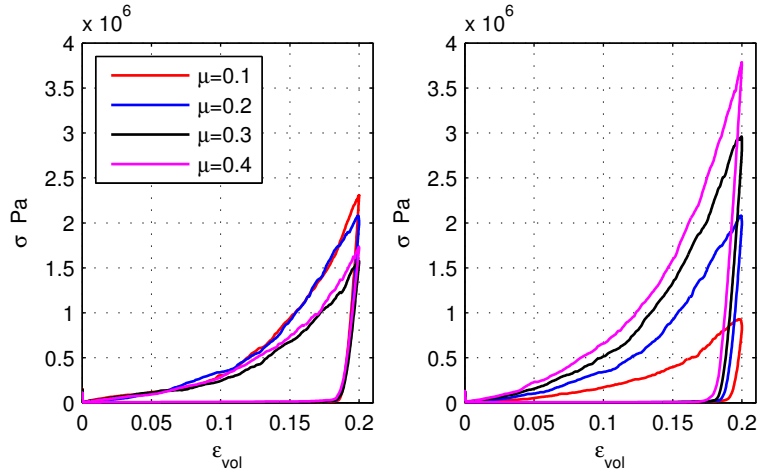

Figure 21: Stress-strain relations during compaction for different friction during preparation (left) and constant friction ($\mu = 0.2$) during preparation (right). The starting volume fraction for the different μ can be found in Table, $k_1 = 10 \cdot 10^5\,\mathrm{N/m}$ for all simulations shown here.

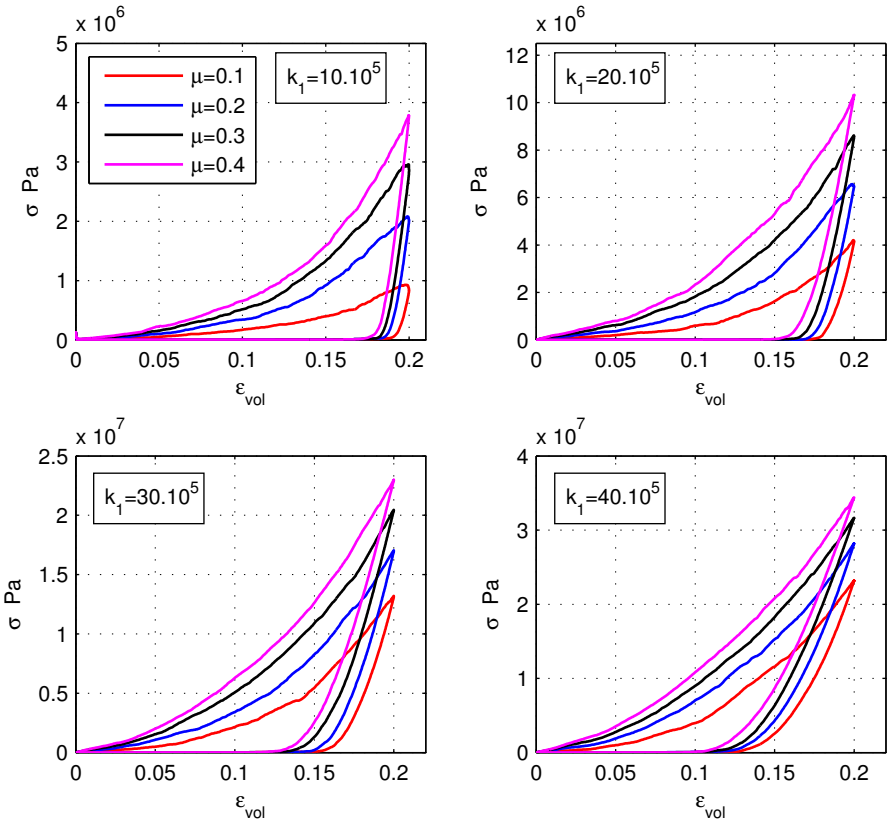

Figure 22: Stress-strain relations during compaction for different μ and k_1. Preparation is performed with the swelling 2 method (see Section 4.2.2) with constant friction $\mu = 0.2$

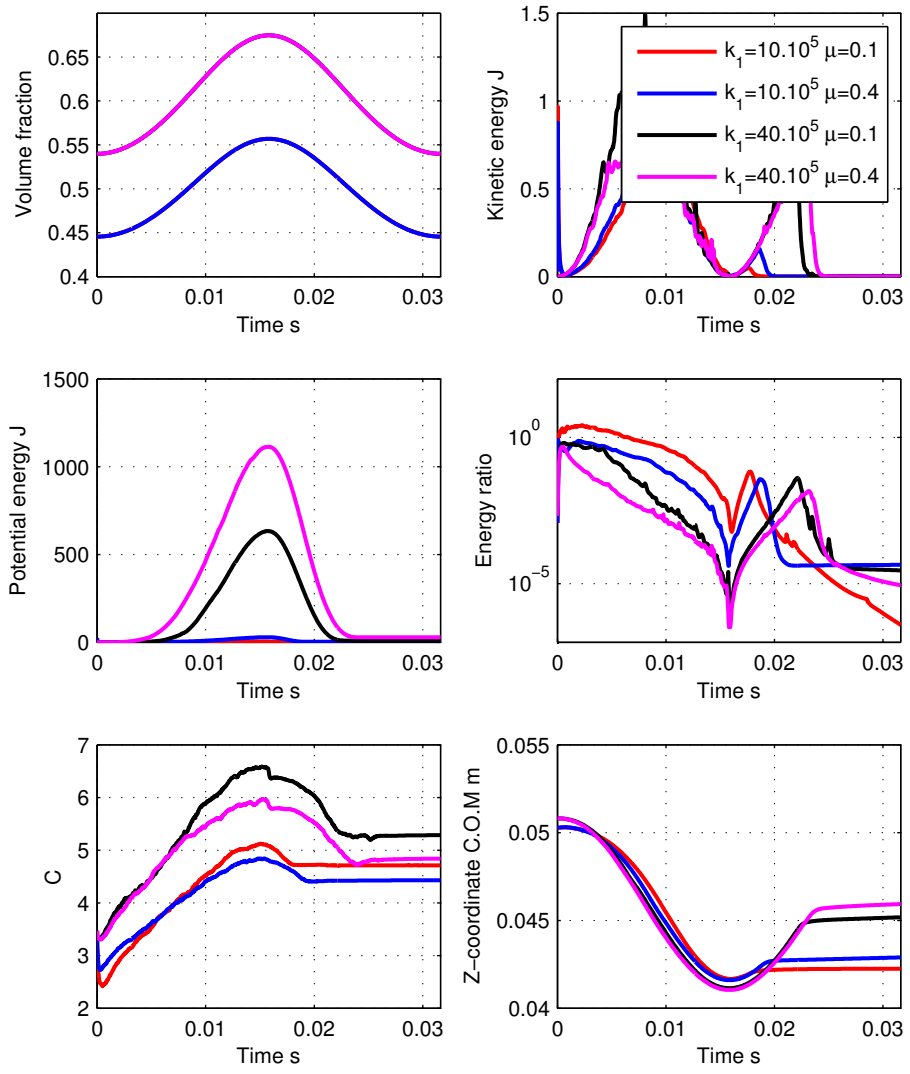

Figure 23: The four extremes of the compaction (see the legend in the left bottom plot). Preparation is performed with the swelling 2 method (see Section 4.2.2) with constant friction $\mu = 0.2$. In samples with higher k_1 more potential energy is built up, these show more elastic recovery, which means less compaction (see the bottom right plot). Lower friction leads to less built up from potential energy and less elastic recovery, which means better compaction.

4.3.3 *Compaction Preparation Pressure Control*

The stress-strain relations during compaction for systems prepared with the pressure control method described in Section 4.2.3 are shown in Figure 24. Remarkably, in these plots is the huge difference in stress between particle systems with $k_1 = 10 \cdot 10^5\,\mathrm{N/m}$ and the other simulations. This

difference is present because the particle systems with $k_1 = 10 \cdot 10^5\,\mathrm{N/m}$ has a significantly lower volume fraction than the others and is therefore much easier to compact. Probably, the particle system has already some initial strength (gathered from the swelling till volume fraction $\nu = 0.425$) in advance of pressure control, this is shown in Figure. In the case of very low k_1 a weak solid state is reached after relaxation and this will affect the pressure control. The swelling before the pressure control is necessary, otherwise the isotropic random condition would not be satisfied. Wall effects would occur: particles will stick to the wall during movement. But the question arises: what volume fraction should be chosen so that an isotropic structure is created and systems show equal initial strength. This question has not been addressed in this research.

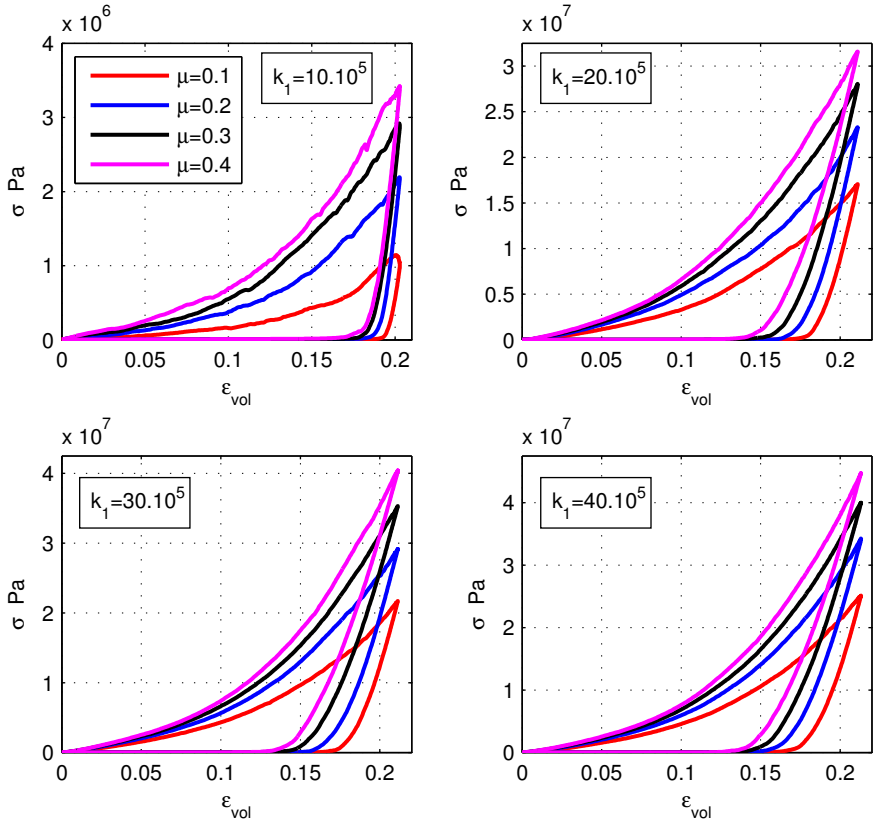

Figure 24: Stress-strain relations during compaction of particle systems prepared with pressure control method (see Section 4.3.3) for different μ and k_1.

4.3.4 *Conclusions Regarding Compaction*

- The shape of the compaction curves shows 2 different regions: a less stiff region $\epsilon_{\mathrm{vol}} < 0.1$ and a much stiffer region for $\epsilon_{\mathrm{vol}} > 0.1$.
- By increasing the stiffness k_1, the difference between these regions becomes vague. This is because (1) the k_1 stiffness approaches the

k_2 stiffness and (2) samples with higher stiffness are denser (higher non-compacted volume fraction) and more difficult to compact.

- An increase in friction is leading to higher stress levels, because (1) the resistance friction force increases with μ and (2) higher friction makes it more difficult for particles to intrude into void spaces. These effects result in less contacts and therefore lead to higher overlap. Consequently, more potential energy is build up and more elastic recovery is present, which has a negative effect on compaction. Therefore, reducing the friction in asphalt mixtures would improve compaction.
- Uniaxial compaction is not leading to an homegenous sample, as the top half of the particle system is more compacted than the bottom half

5 COMPARING SIMULATIONS WITH EXPERIMENTS

This Chapter is dedicated to compare the DEM compaction simulations (see Section 4.3.2) with the experimental tests (see Section 2.3). First, the dimensional analysis and the scaling procedure is explained in Section 5.1 and performed in Section 5.2. Next, the stress-strain behaviour in DEM simulations and experimental tests is compared (Section 5.3) and model parameters are varied (Sections: 5.3.3, 5.3.4 and 5.3.5), in order to investigate the effects and improve the fit between simulations and experiments. After this, in Section 5.4 the influence of different strain rates during compaction is investigated. Finally, compaction is performed in multiple steps (Section 5.5), followed by conclusions regarding this chapter.

5.1 DIMENSIONAL ANALYSIS

The DEM model used in this research, like those in most other simulations codes, do not have a built-in unit system. Any number used is dimensionless and becomes dimensional when it is scaled with the proper fundamental units. Therefore, it is the user's responsibility to ensure that the chosen units are consistent, which means that derived units can be expressed in terms of the fundamental units without conversion factors. The fundamental units of interest for this research, expressed in the SI-system are:

- Mass m_u, specified in kilograms kg
- Length x_u, specified in meters m
- Time t_u, specified in seconds s

The used DEM model in this research is consistent, which means that all model parameters and input data, are expressed in terms of the fundamental units: m_u, x_u and t_u. However, the numerical magnitude of most quantities is not specified a-priori and can be chosen freely. After choosing realistic sizes and masses for the particles in DEM simulations (see Section 2.5) the fundamental units $m_u = 1\,\text{kg}$ and $x_u = 1\,\text{m}$ are fixed, so the sizes and masses correspond more or less to the physical aspects of the mixture. The unit of time t_u is not yet defined; this time unit, is used for scaling the stress level upwards, in order to match the experimental measurements, see the next Section 5.2. Consequently, the unscaled parameters become realistic, dimensional quantities after scaling.

5.2 PARAMETER SCALING

In the first DEM simulations most model parameters were freely chosen. Except parameters that where depending on density or length scales; these were already based on realistic physical aspects of the asphalt mixture. Fortunately, it followed that the shape of the stress-strain of DEM results was in good qualitative agreement with the experimental tests (and can be matched even better by changing some model parameters slightly). If the stress level was scaled-up, with a constant factor. This stress up-scaling is possible by adapting t_u, because the unit of stress is defined as:

$$\sigma_u = \frac{\text{Force}}{\text{Area}} = \frac{\text{Mass} \cdot \text{Acceleration}}{\text{Length} \cdot \text{Length}} = \frac{m_u \cdot \frac{x_u}{t_u^2}}{x_u^2} = \frac{m_u}{x_u t_u^2} \tag{24}$$

And if for example t_u is scaled-up with a factor of $\sqrt{\frac{1}{10^5}} \approx 0.0032$, then the stress levels are increased with a factor of 10^5, due to Equation 24. This means that all model parameters or input data which are depending on time must be scaled with this factor when expressed dimensional. This is explicitly done below for some quantities (the dimensionless variables are indicated by an apostrophe):

- The dimensional stiffness k_2, defined in $\frac{\text{kg}}{\text{s}^2}$ becomes:

$$k_2 = k_2' \cdot \frac{m_u}{t_u^2} = k_2' \cdot \frac{1}{\left(\sqrt{\frac{1}{10^5}}\right)^2} \frac{\text{kg}}{\text{s}^2} = k_2' \cdot 10^5 \frac{\text{kg}}{\text{s}^2} \tag{25}$$

- The dimensional viscosity γ, defined in $\frac{\text{kg}}{\text{s}}$ becomes:

$$\gamma = \gamma' \frac{m_u}{t_u} = \gamma' \cdot \frac{1}{\left(\sqrt{\frac{1}{10^5}}\right)} \frac{\text{kg}}{\text{s}} = \gamma' \cdot \sqrt{10^5} \frac{\text{kg}}{\text{s}} \tag{26}$$

- The dimensional simulation time T_{DEM}, defined in s becomes:

$$T_{\text{DEM}} \quad = \quad T'_{\text{DEM}} \cdot t_u = 10 \cdot \sqrt{\frac{1}{10^5}}\,\text{s} \tag{27}$$

- The dimensional time step Δ_t, defined in s:

$$\Delta_t = \Delta_t' \cdot t_u = 1 \cdot 10^{-4} \cdot \sqrt{\frac{1}{10^5}}\,\text{s} \tag{28}$$

- The dimensional starting velocities v, defined in $\frac{\text{m}}{\text{s}}$:

$$v = v' \cdot \frac{x_u}{t_u} = v' \cdot \frac{1}{\sqrt{\frac{1}{10^5}}} = v' \cdot 312.5 \frac{\text{m}}{\text{s}} \tag{29}$$

Property	Symbol	Dimensionless	Dimensional	SI units
Length Unit	x_u	1	1	m
Mass Unit	m_u	1	1	kg
Time Unit	t_u	1	$\sqrt{\frac{1}{10^5}}$	s
Average Radius	$\bar{R}$	0.004	0.004	m
Material density	ρ	2000	2000	kg/m^3
Elastic stiffness	$k = k_2$	100	$100 \cdot 10^5$	kg/s^2
Plastic stiffness	k_1/k_2	1/10,2/10,3/10,4/10	1/10,2/10,3/10,4/10	-
Adhesion stiffness	k_t/k_2	1/5	1/5	-
Friction stiffness	k_s/k_2	1/5	1/5	-
Plasticity range	ϕ	0.1	0.1	-
Coulomb friction	$\mu = \mu_s = \mu_d$	0.1, 0.2, 0.3, 0,4	0.1, 0.2, 0.3, 0,4	-
Normal viscosity	$\gamma = \gamma_n$	0.001	0.3125	kg/s
Tangential viscosity	γ_t/γ	10	10	-
Background viscosity	γ_b/γ	10	10	-
Background torque	γ_{br}/γ	10	10	-

Table 6: Model parameters DEM; as used in both preparation and compaction, the averaged radius is based on the reached volume fraction after preparation (in this table the averaged radius is based on the preparation method swelling 1 (Section 4.2.1)). First and second column define the meaning of the symbols. The third column are the (un-scaled, dimensionless) numbers used in DEM. The fourh column are the (scaled, dimensional) physical quantaties in SI-units, which can appropriately scaled by time t_u.

- The dimensional growth rate g_r, defined in $\frac{1}{s}$:

$$g_r = g_r' \cdot \frac{1}{t_u} = 0.1 \cdot \frac{1}{\sqrt{\frac{1}{10^5}}} \frac{1}{s} \tag{30}$$

The dimensional and dimensionless parameters and variables are given in the third and fourth column of Table 6 respectively. In order to investigate if stress levels were consistently and properly increased by scaling with t_u, a preparation- and compaction simulation was performed with both dimensional and dimensionless numbers, as shown in Figure 25. It followed that stress levels were perfectly corresponding, as well as other particle characteristics; such as the energy ratio and the number of contacts. So, in conclusion it is proven that the scaling is providing the same results as a simulation using unscaled parameters As result of the scaling procedure

the strain rate has changed. The new dimensional strain rate $\dot{\epsilon}$, defined in $\frac{1}{\mathrm{s}}$ is:

$$\begin{aligned} \dot{\epsilon}_{\mathrm{DEM}} &= \dot{\epsilon}'_{\mathrm{DEM}} \cdot \frac{1}{t_u} = \dot{\epsilon}'_{\mathrm{DEM}} \cdot \frac{1}{\sqrt{\frac{1}{10^5}\,\mathrm{s}}} = \dot{\epsilon}'_{\mathrm{DEM}} \cdot 312.5\,\frac{1}{\mathrm{s}} \\ &= \frac{v_{\mathrm{wall}}}{L_0} \cdot 312.5\,\frac{1}{\mathrm{s}} = \frac{\frac{0.02}{5}}{0.1} \cdot 312.5\,\frac{1}{\mathrm{s}} = 12.5\,\mathrm{s}^{-1} \end{aligned} \tag{31}$$

The strain rate in the experiments equals:

$$\dot{\epsilon}_{\mathrm{exp}} = \frac{v_{\mathrm{press}}}{l_0} = \frac{0.00087\,\frac{\mathrm{m}}{s}}{0.065\,\mathrm{m}} = 0.0134\,\mathrm{s}^{-1} \tag{32}$$

So the strain rate in the simulations is of order 10^3 higher than the strain rate in the experiments. This can be adapted by changing the period of the wall motion during compaction. A longer period of 10^3, meaning the new simulation time: $T_{\mathrm{DEM}} = 10^4 t_u$, would then compare with the strain rate in the experiments. This is partly done in section 5.4, where the strain rate is increased with a maximum factor of 10^2. Since this rate did not differ much with the simulation where the rate was increased with factor 10^2, one can assume to be already in the quasi-static regime and postpone a more detailed study of rate effects to further research. However, a simulation with exactly the same strain rate as used in the experiments would take about 7 days CPU-time, this is not feasible, taken into account the many simulations performed in this research.

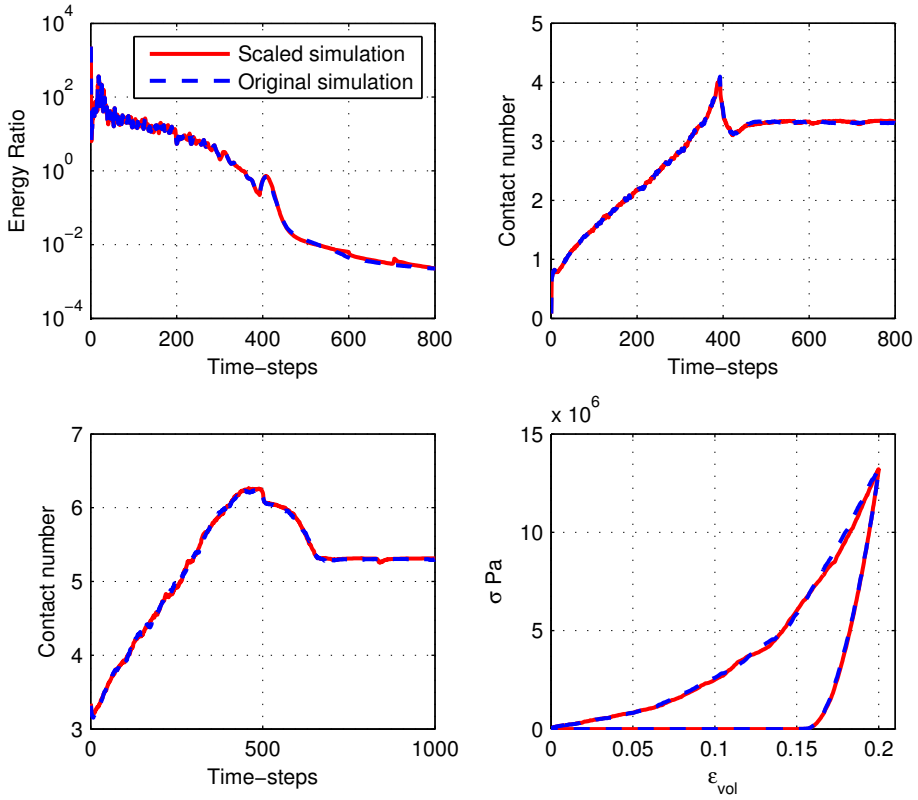

Figure 25: Characteristics of a swelling simulation (top) and a compaction simulation (bottom); preparation is performed with the swelling 2 method (see Section 4.2.2), $k_1 = 30 \cdot 10^5\,\mathrm{N/m}$, $\mu = 0.2$. Blue dashed line: the (un-scaled, dimensionless) simulation (for model parameters see column 3 in Table 6). Red line: scaled (scaled, dimensional) simulation (for model parameters see column 4 in Table 6). A good match is obtained between the original and the scaled simulation; see the Energy ratio plot (top left) and contact number plots (top right and bottom left). The stress levels (bottom right plot) match the experimental results (see Figure 26, bottom right plot), if the stress is scaled with a factor of 10^5. The dimensional data matches directly after scaling all parameters with the appropriate units. This figure confirms that scaling up stress levels with a factor 10^5 is allowed, if time-scale is adapted accordingly.

5.3 OPEN ASPHALT

As explained in earlier in Section 4.1 the defined modelling assumptions compare best with an open asphalt mixture; therefore, it was chosen to compare DEM results results with the experimental compaction results of an open asphalt mixture. Compaction results of samples prepared with swelling 2 method (see Section 4.3.2) are used, because this preparation methods is considered to be the best.

In Figure 26 the stress-strain relations for variable k_1 and μ (see the legend) are compared with the stress-strain curves from the experimental tests; the lines called "Oil" and "Bit" (Oil means "fake bitumen" and "Bit" means real bitumen as used in the mixture). The stress in these simulations is scaled with a factor of 10^5 and accordingly the time-scale is changed, which is allowed; see Section 5.2. From these plots can be concluded that the simulation results with the lowest and highest elastic stiffness ($k_1 = 10 \cdot 10^5$ N/m; $40 \cdot 10^5$ N/m), are strongly deviating from the experimental results. In the following two Sections (5.3.1 and 5.3.2) the bitumen- and oil-sample will be compared with the DEM results

5.3.1 *Bitumen Sample*

The bitumen sample matches the "$k_1 = 20 \cdot 10^5$ N/m, $\mu = 0.4$" simulation (top right plot Figure 26) and (even better) the "$k_1 = 30 \cdot 10^5$ N/m, $\mu = 0.1$" simulation (middle left plot Figure 26). The question arises whether the friction or the stiffness parameter describes the correct behaviour. In the left bottom plot in Figure 26 these simulations are compared. It appears that the best fit is obtained with the "$k_1 = 30 \cdot 10^5$ N/m, $\mu = 0.1$ simulation. The determination of realistic friction parameters was not possible in this research, therefore this parameter cannot be addressed to the used bitumen in the mastic. However, the influence of friction in compaction simulations is further studied in Section 5.3.5.

5.3.2 *Oil Sample*

The oil-sample follows the "$k_1 = 20 \cdot 10^5$ N/m, $\mu = 0.1$" simulation in the less stiff region (for $\epsilon_{vol} < 0.1$) and is approximating the "$k_1 = 20 \cdot 10^5$ N/m, $\mu = 0.2$" simulation for higher strain levels, see Figure (26). To improve the fit and gain a better understanding of model parameters, the influence of the following parameters were further researched: k_1, k_2 and μ, see the Sections 5.3.3, 5.3.4 and 5.3.5. The "$k_1 = 20 \cdot 10^5$ N/m, $\mu = 0.1$" compaction simulation is in these analyses used for reference and from now on named as the reference simulation. The following analyses were performed:

- An increase of k_2 stiffness, see Section 5.3.3. It is thought that this will scale the stress-strain upwards for higher strain levels, as it is assumed that for higher strain levels the k_2 stiffness will be dominant and higher k_2 will lead to stiffer behaviour.
- An increase of k_1 stiffness, see Section 5.3.4. It is thought that this parameter scales the whole curve upwards, which may improve the fit.
- An increase of friction μ, see Section 5.3.5. It is thought that by performing simulation with variable μ (between 0.1 and 0.2), the match with the experiments will be improved.

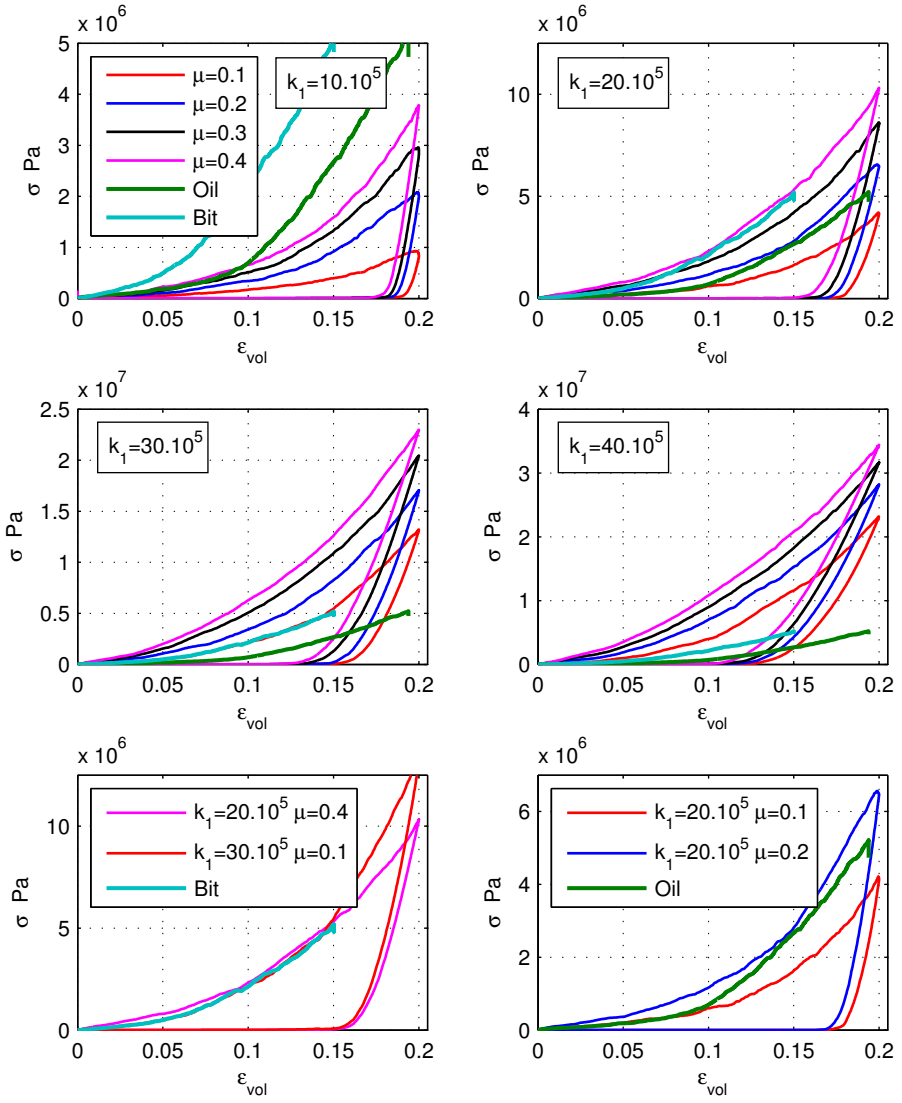

Figure 26: Stress-strain relations during DEM- and experimental compaction. The top four plots show the effect of different loading stiffness k_1 and friction μ during compaction. In the two bottom plots the up to now best match with the experimental tests (the Oil- and Bit-curves) is given. The experimental bitumen sample is already in good agreement with the $k_1 = 30 \cdot 10^5\,\mathrm{N/m}$, $\mu = 0.1$ simulation. In order to improve the fit between the oil sample and the model results further analyses were performed, as explained in Section 5.3.2

5.3.3 *Influence of k_2*

It has been investigated if an increase in k_2 matches the experimental oil-sample better than the reference simulation, because if the region for $\epsilon_{\mathrm{vol}} >$

0.1 from the reference simulation could be scaled upwards a better fit is obtained. For larger deformations (overlap $\delta > \delta^*$), the k_2 parameter affects the loading behaviour. Therefore, it is assumed that this parameter affects the compaction at larger strain levels, which is exactly what is wanted. To investigate this assumed influence, a set of new simulations with variable k_2 were executed. The results are shown in Figure 27. It can be seen that k_2 influences the second region $\epsilon_{\text{vol}} > 0.1$ (slightly) and that there is almost no difference in the first region.

An increase of k_2 with a factor of 2, increases the stress with a factor of only 1.12 (at maximum strain). Therefore, the effect of k_2 is small and thus negligible for now. The reason for this could be a too small averaged contact overlap, what physically means that no stone-stone interactions are present. This has been confirmed in a contact analysis: all contacts were plotted as small dots, with as x-coordinate the overlap δ, and as y-coordinate the normal contact force f_n, see Figure 28. The black dashed lines are representing the loading/unloading lines in the adhesive contact model (as shown in Figure 11). The overlap from k_1 to k_2 is based on the averaged radius multiplied by ϕ, which gives the average size of the plastic range (see Equation 2). By plotting these contacts, it is possible to determine whether contacts are in the plastic region: $\delta < \delta^*$where loading/unloading occurs with k_1 or k_2 (this physically represents mastic-mastic interaction), or the elastic region: $\delta > \delta^*$ and loading/unloading occurs with k_2^* (which represents stone-stone interaction).

This analysis was performed at 4 different moments during compaction of the reference simulation "$k_1 = 20 \cdot 10^5\,\text{N/m}$, $\mu = 0.1$": (1) at the start of compaction $t = 0$, (2) during compaction $t = 4$, (3) at maximum compaction $t = 5$, and (4) at the end of compaction $t = 10$. At the start of compaction almost all contacts are in the k_1 zone (possibly even all contacts, because the overlap k_1 to k_2^* is based on the averaged radius); subsequently, compaction is started, some contacts are in the elastic region, but the majority is in the plastic region. This analysis confirms that few contacts are in the elastic region, and that therefore the influence of k_2^* is small. k_2^* will probably be influential if the volume fraction is increased, meaning that particles cannot occupy void space anymore and loading directly leads to higher overlap. Alternatively, if the ϕ parameter would be taken smaller, the elastic region is reached earlier and the k_2^* stiffness will have greater effect. However, this has not been examined in this research.

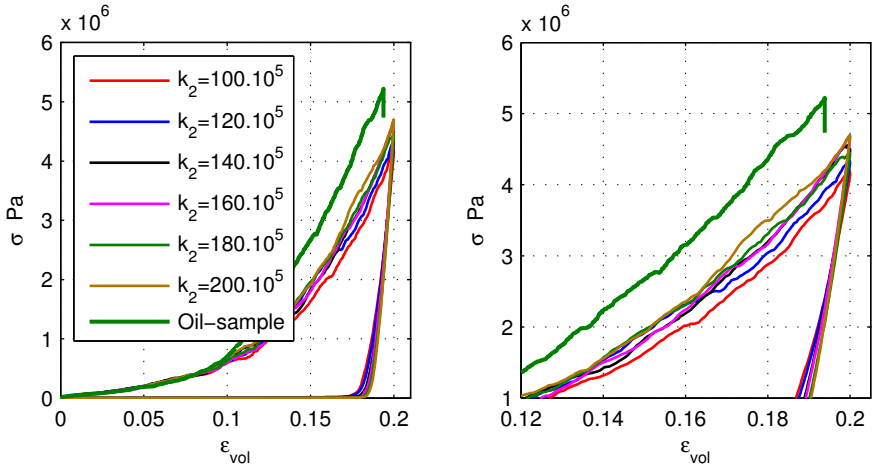

Figure 27: Stress-strain relations during compaction with variable k_2^*, see the legend. Increasing k_2^* has not much influence during loading in comparison with the reference simulation (red line). Note that k_2^* also affects the unloading: with higher k_2^* the slope during unloading (k_2) is steeper and unloading stiffness is higher, see Equation 19), resulting in less elastic recovery.

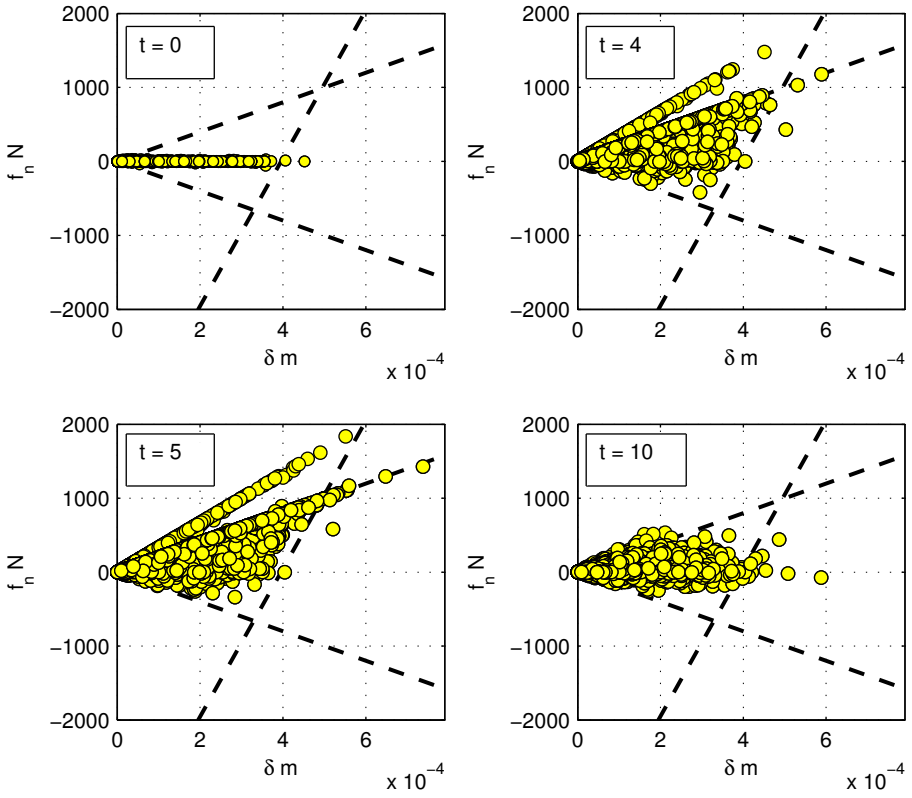

Figure 28: Representation of all the contacts during compaction of the reference simulation, contacts presented as yellow dots and are visualized by plotting f_n versus δ. In this way the position of the contact compared to the contact model is given. The black dashed lines represents the loading and unloading lines from the contact model, given in Figure 11; the slope of these lines is based on model parameters from the reference simulation.

5.3.4 *Influence of k_1*

It has been investigated if an increase in k_1 matches the experimental oil-sample better than the reference simulation. Since k_1 strongly dominates the preparation process (see Section 4.2.2), different initial states for variable k_1 have been made in order to get an equal starting pressure (see Section 4.3.2).

The results are shown in stress-strain relations in Figure 29. From these plots can be seen that with an increased stiffness of $k_1 = 22 \cdot 10^5\,\mathrm{N/m}$, a reasonable fit is obtained. The starting volume fraction of this simulation (after preparation) is increased to $v_0 = 0.496$ (in the reference simulation: $v_0 = 0.485$, see Table 5). Increasing k_1 means in physical terms: higher stiffness of the mastic and numerically: the system is more dense.

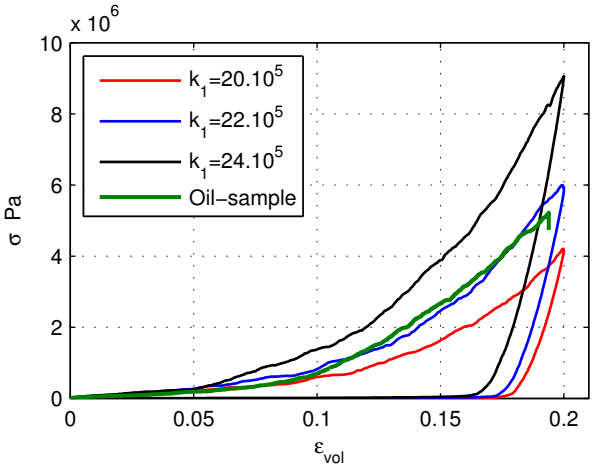

Figure 29: Stress-strain relations during compaction. Red line: the reference simulation; green line: the experimental oil-sample and DEM simulations with variable k_1 as defined in the legend (other simulation parameters equal the reference simulations). By increasing k_1 (N/m), the fit with the experimental oil-sample becomes better.

5.3.5 *Increased Friction*

It has been investigated if an increase in μ matches the experimental oil-sample better than the reference simulation. This was been studied by performing a range of simulations with different friction coefficients, the results are plotted in Figure 30. From this plot can be concluded that an increase in friction is scaling the whole stress-strain curves upwards. However, the discrepancy with the oil-sample remains and cannot be fitted by only changing μ. It can be concluded that by changing the friction, the magnitude of the stress-strain curve can be tuned, but not its shape.

5.3.6 *Conclusions Parametric Analysis*

In summary the following can be said about the the influence of k_1, k_2 and μ during compaction:

- By changing k_1 the shape of the stress-strain curve can be changed; this is the most important parameter for improving the fit between DEM- and experimental results.
- The influence of k_2 is small during compaction.
- Higher k_2 is leading to less elastic recovery.
- By changing μ, the stress-strain curve can be scaled over the whole length, but this does not affect the shape of the curve.

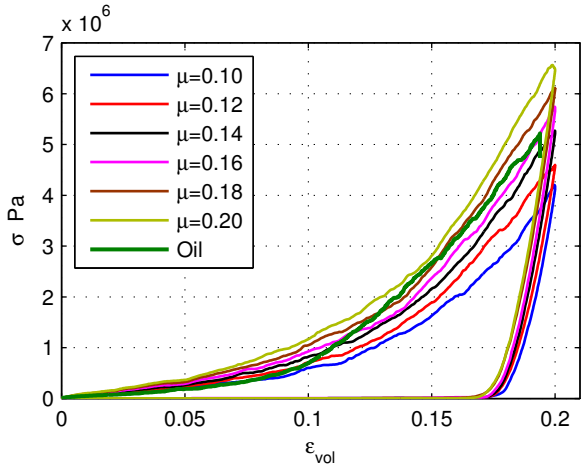

Figure 30: Stress-strain relations during compaction. Blue line: the reference simulation; green line: the experimental oil-sample and DEM simulations with variable μ defined in the legend (other DEM parameters equal the reference simulations). By increasing μ the whole stress strain curve is scaled upwards and the discrepancy with the oil sample remains.

5.4 INFLUENCE OF STRAIN RATE

The stress-strain behaviour during compaction is dictated by the motion of the top wall. This wall moves with a co-sinusoidal shape downwards with an amplitude of 0.02 m and period $10 \cdot \sqrt{\frac{1}{10^5}}$ s. Resulting in a maximum strain of $\epsilon_{\text{vol}} = 0.2$. The influence of different strain rates is studied by changing the period length of the top wall motion, as this affects the compaction velocity and the strain rate, see Equation 31. The wall motion in this formula is assumed linear. This strain rate in the DEM compaction simulations is $\dot{\epsilon}_{\text{DEM}} = 12.5\,\frac{1}{\text{s}}$, is about 10^3 times higher than the strain rate in the experiments $\dot{\epsilon}_{\text{exp}} = 0.0134\,\frac{1}{\text{s}}$. For simplicity, the strain rate in DEM simulations is taken much lower, because a simulation with realistic strain rate ($\dot{\epsilon}_{\text{exp}}$) would take approximately 7 days CPU-time, this is not feasible, taken into account the many simulations performed in this research.

However, some research was performed with an increased strain rate, by increasing the period of the downward motion of the top wall; these results are shown in Figure 31, where the stress-strain relations are shown for a normal simulation $T_{\text{DEM}} = 10 \cdot t_u \approx 0.0316\,\text{s}$, two longer simulations (T $=10 \cdot T_{\text{DEM}}$ and T $=100 \cdot T_{\text{DEM}}$) and a shorter simulation (T $=0.1 \cdot T_{\text{DEM}}$). The simulation with lower strain rate (T $=0.1 \cdot T_{\text{DEM}}$) has a negative influence on compaction: stress levels are significantly higher. Compaction with a higher strain rate (T $=10 \cdot T_{\text{DEM}}$ and T $=100 \cdot T_{\text{DEM}}$) is leading to better compaction, especially in the middle region ($\epsilon_{\text{vol}} = 0.05 - 0.15$), where the strain rate is most influential (since the wall motion is sinusoidal), stress levels are significantly lower.

The simulation with the increased strain rate (T $=10 \cdot T_{\text{DEM}}$) does not differ much with the highest strain rate simulation (T $=100 \cdot T_{\text{DEM}}$). There-

fore, it can be concluded that the simulation with the highest strain rate is (almost) quasi-static.

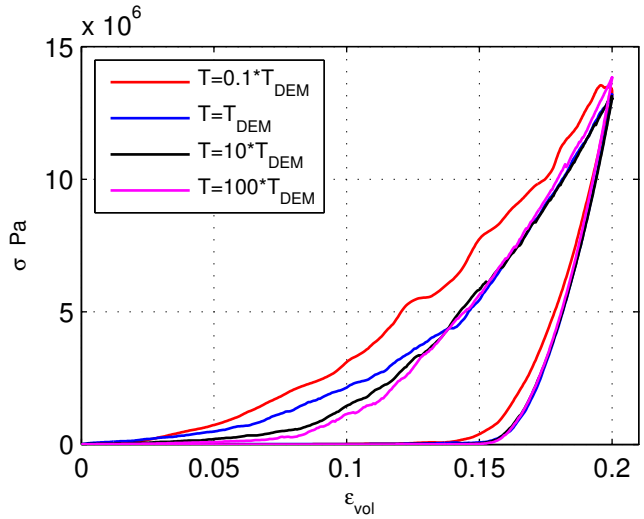

Figure 31: Stress-strain relations during DEM compaction with different strain rates; $k_1 = 30 \cdot 10^5\,\mathrm{N/m}$, $k_2 = 100 \cdot 10^5\,\mathrm{N/m}$, $\mu = 0.1$. The blue line conforms the strain rate used during compaction in this research. A higher strain rate has a positive influence on compaction (the black and magenta lines). The simulation with the highest strain rate is assumed (almost) quasi-static.

5.5 MULTIPLE STEPS COMPACTION

In the real world compaction takes place in multiple steps: rollers are passing several times over the asphalt and in the laboratory, the hammer from the Marshall tests is hitting the asphalt mixture multiple times. After calibration of DEM parameters with the simple compaction experiment. DEM can now be used to study the influence of multiple steps in the simulation of compaction.

This is done by dividing the top wall displacement into 10 increments. The period stayed the same $T_{\mathrm{DEM}} = 10 \cdot t_u \approx 0.0316\,\mathrm{s}$, but the amplitude was increased by increments of 0.002. This has been performed for the "$k_1 = 30 \cdot 10^5\,\mathrm{N/m}$, $\mu = 0.1$" simulation. Results from incremental compaction were compared with a normal simulation of compaction, where the same model parameters as used during incremental compaction, but the strain rate was decreased ($T_{\mathrm{DEM}} = 100 \cdot t_u \approx 0.316\,\mathrm{s}$).

The stress-strain relations for these simulations and other simulation characteristics are presented in Figures 32 and 33. It can be seen that the incremental compaction is leading to lower stress levels. During the first increments (1 - 5) not much potential energy (or contact overlap) is built up: particles can reorganize. In the second region (say increment 6 and above) more potential energy is built up: the bitumen layer around the particles is pressed together, resulting in remaining potential energy.

Remarkable is the strange shape of the first part of stress-strain curve during incremental compaction, a possible explanation is given in the caption from Figure 34.

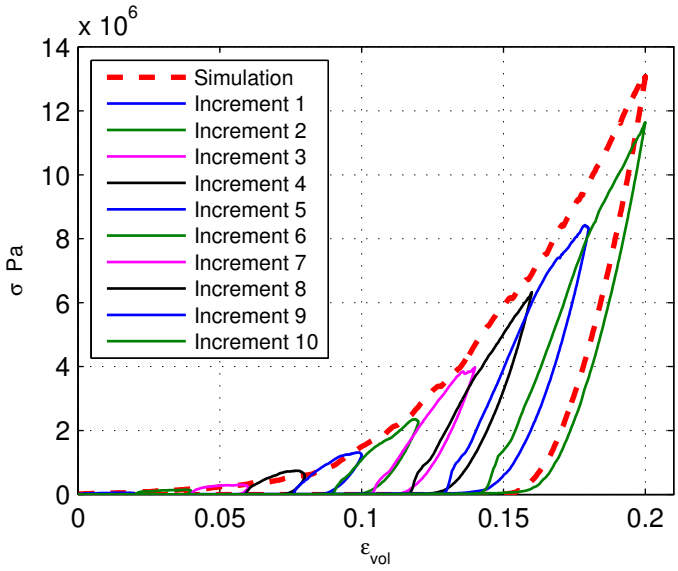

Figure 32: Stress-strain relations during incremental compaction (the solid lines) and ordinary compaction (red-dashed line). Incremental compaction is leads to lower stress levels. Each simulation with the incremental compaction as a strain rate $\dot{\epsilon}_{\text{DEM}} = 12.5\,\frac{1}{\text{s}}$ ($T_{\text{DEM}} = 10 \cdot t_u$) and the ordinary compaction has a decreased strain rate $\dot{\epsilon}_{\text{DEM}} = 1.25\,\frac{1}{\text{s}}$ ($T_{\text{DEM}} = 100 \cdot t_u$)

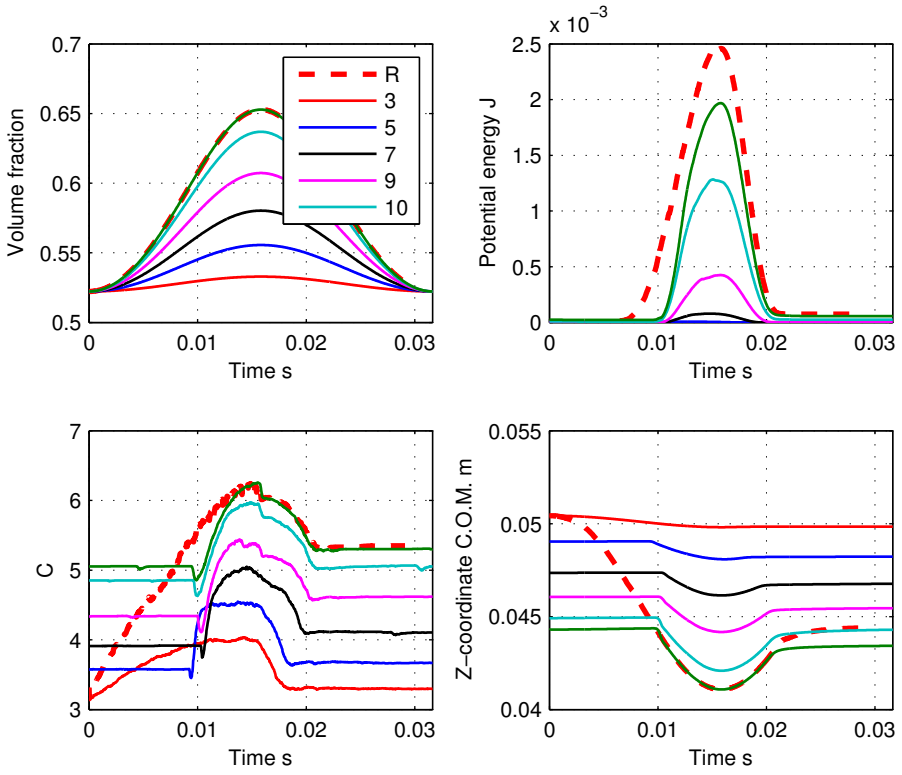

Figure 33: Characteristics of incremental compaction (the solid lines, $\dot{\epsilon}_{\text{DEM}} = 12.5\,\frac{1}{s}$) and normal compaction (with increased strain rate, $\dot{\epsilon}_{\text{DEM}} = 1.25\,\frac{1}{s}$); the red-dashed line, note that the time scale on the x-axes of the plots, is not correct for this simulation (need to be multiplied with 10). The incremental compaction is leading to lower stress levels. During the first increments (1 - 5) not much potential energy (or contact overlap) is built up: particles can reorganize. In the second region (say step 6 and above) more potential energy is built up: the bitumen layer around the particles is pressed together, resulting in remaining potential energy

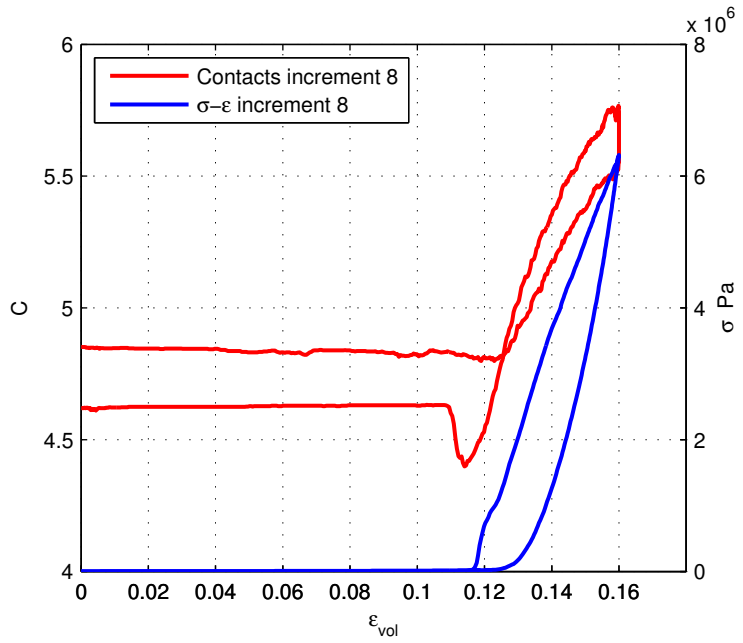

Figure 34: Stress-strain relation (blue line) and number of contacts (red line) plotted versus strain during incremental compaction (increment 8, see Figure 32). During incremental compaction, firstly contacts are broken (see the valley in the contacts plot), then the stress on the bottom wall starts rising, with an initial different slope. Possibly, the wall motion leads to reorganization of particles (the valley in the contact plot curve, which not affects the stress on the bottom wall) and when reorganization is not possible anymore the stress starts rising.

5.6 CONCLUSIONS

- With the meso-sale DEM model it is possible to model stress-strain behaviour of asphalt mixtures under uniaxial loading.
- The upwards stress scaling with a factor of 10^5 is allowed by adapting the unit of time. Accordingly, the non-dimensional numbers become dimensional quantities.
- It appeared that the plastic stiffness k_1 is dominant for shape and magnitude and that the influence of k_2 is small. Note that this is depends on v (volume fraction) and ϕ (plasticity range): for higher volume fraction or lower plasticity range, the k_2 region will be earlier reached and might affect the stress-strain behaviour. However, this is not been investigated in this research.
- With use of the time-tuned stiffness parameter k_1 and the educated guess for ϕ, the mastic can be modelled.
- The samples which are denser during preparation with $k_1 > 30$, deviate from the experimental tests: probably here are initially more

contacts present with larger overlap and this leads immediately to stiff behaviour; this has also not further been studied in this research.

- If a model is desired that is capable modelling different behaviour with k_1 and k_2, then the plasticity range parameter ϕ must be taken lower. The k_2 region will then be reached earlier.
- Realistic friction parameters must be derived from other kind of tests; however, it must be noted that μ is not related to mastic/aggregate friction only, but also includes shape and disorders in actual mixtures.
- The best parameters that match the experimental bitumen-sample are: $k_1 = 30 \cdot 10^5$, $k_2 = 200 \cdot 10^5$, $\mu = 0.1$ (for more parameters see Table 6, column 3)
- The best parameters that match the experimental oil-sample are: $k_1 = 22 \cdot 10^5$, $k_2 = 200 \cdot 10^5$, $\mu = 0.1$ (for more parameters see Table 6, column 3)

6 CONTINUUM MODEL

In the first part of the research asphalt compaction has been simulated with discrete element modelling. This Chapter tries to link these simulations with a continuum model that can be applied on the macro-scale. For this purpose the Cam Clay material model available in Abaqus (FEM program), has been chosen, because it is often used to describe the compaction of soils, foundations and granular materials. In this chapter only the basic theory behind the Cam Clay model is explained; for a detailed description see Wood [18]. For determining model parameters of the Cam Clay model, calibration tests have to be performed. In practice, these tests are hard to perform and require expensive testing equipment. In this research calibration tests are performed with the use of DEM and result are used as input in the Cam Clay model. If this leads to successful modelling with FEM, i.e. the same behaviour as in uniaxial compaction with DEM is obtained, a huge amount of time and costs are saved, as no actual calibration tests are necessary and the modelling on the macro-scale is made possible.

6.1 CAM CLAY MATERIAL MODEL

The cam clay model is used in soil mechanics. It accommodates for large volumetric changes and it is possible to apply self defined hardening behaviour. With these properties it is investigated, if the same behaviour as in the modelling of uniaxial compaction with DEM, can be obtained. The following applies for the Cam Clay model provided in Abaqus (as described in the Abaqus user manual [1]):

- It describes the inelastic behaviour of the material by a yield function that depends on the three stress invariants.
- An associated flow rule is assumed to define the plastic strain rate.
- It involves a strain hardening theory that changes the size of the yield surface according to the inelastic volumetric strain.
- The elastic part of deformation is defined by a linear elastic material model.
- The hardening law must be defined piecewise linear or in an exponential form.

6.1.1 *Yield Surface*

The model is based on the yield surface, which is described in the $p - t$ plane given by Equation 33. It is assumed that the yield locus has an

elliptical shape passing through the origin in this plane, as displayed in Figure 35.

$$\begin{cases} \text{for } p > a & \frac{1}{\beta^2}\left(\frac{p}{a}-1\right)^2 + \left(\frac{t}{Ma}\right)^2 - 1 = 0 \\ \text{for } p \leq a & \left(\frac{p}{a}-1\right)^2 + \left(\frac{t}{Ma}\right)^2 - 1 = 0 \end{cases} \tag{33}$$

Where p is the equivalent pressure stress defined as:

$$p = -\frac{1}{3}\left(\sigma_{ii}\right) \tag{34}$$

q is the Mises equivalent stress, defined as:

$$q = \sqrt{\frac{3}{2}S : S} = \sqrt{\frac{\left(\sigma_1-\sigma_2\right)^2 + \left(\sigma_2-\sigma_3\right)^2 + \left(\sigma_1-\sigma_3\right)^2}{2}} \tag{35}$$

t is a deviatoric stress measure:

$$t = \frac{q}{g}$$

g is used to shape the yield surface in the deviatoric plane ($\sigma_1 + \sigma_2 + \sigma_3 = 0$), g is defined as:

$$g = \frac{2K}{1 + K + (1-K)\left(r/q\right)^3} \tag{36}$$

r is the third stress invariant defined as:

$$r = \left(\frac{9}{2}S : S \cdot S\right)^{\frac{1}{3}} \tag{37}$$

Where S is the deviatoric stress tensor:

$$S = s_{ij} = \sigma_{ij} - p\delta_{ij} \tag{38}$$

An associated flow rule is used in this model. The size of the yield surface is defined by a:

$$a = \frac{p_c}{(1+\beta)} \tag{39}$$

This parameter characterizes hardening or softening behaviour. The evolution of this parameter is in this research defined as a piecewise linear function, relating the yield stress in hydrostatic compression p_c with the corresponding volumetric plastic strain $\epsilon_{\text{vol}}^{\text{pl}}$. These assumptions introduce the following Cam Clay model parameters to describe plastic deformation: M, K, β, $\epsilon_{\text{in}}^{\text{pl}}$ and $p_c\left(\epsilon_{\text{vol}}^{\text{pl}}\right)$:

- M is the slope of the critical state line in the $p-t$ plane (the ratio of t to p at critical state). The term "critical state" is used to describe the state of the system which is able to continue shearing to large strains without changing stresses or density. From triaxial compression tests in DEM followed $M \approx 0.6$; see Section 6.3.

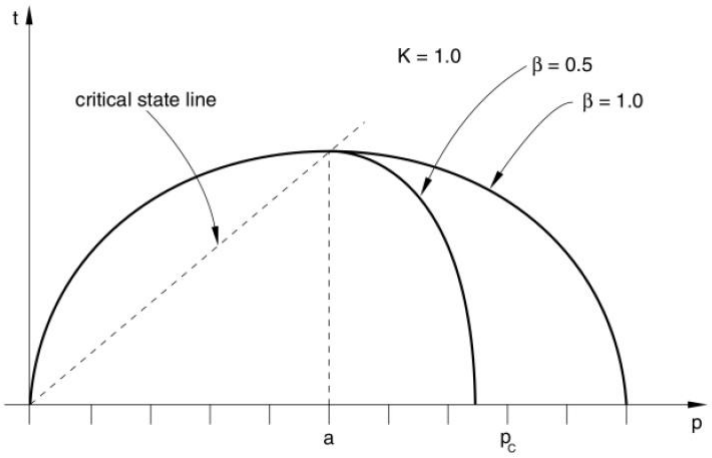

Figure 35: The cam-clay yield surface in the $p-t$ plane.

- K is the ratio of the flow stress in triaxial tension to the flow stress in triaxial compression. If $K = 1$, then $g = 1$ and $t = q$. Then, the yield surface then does not depend on the third stress invariant, which results in an circle shaped yield surface in the deviatoric plane.
- β is a parameter that determines the slope on the "wet" size of the critical state line, investigations in order to obtain realistic values for this parameter, has not been performed in this research.
- $\epsilon_{\text{in}}^{\text{pl}}$ is the strain level from as plastic deformation occurs. This parameter is chosen very low $\epsilon_{\text{in}}^{\text{pl}} = 1 \cdot 10^{-5}$, doing so, the elastic behaviour is almost negligible.
- $p_c\left(\epsilon_{\text{vol}}^{\text{pl}}\right)$ prescribes the size of the yield function as function of the plastic strain. This data was determined from a hydrostatic compression test and given in tabular form to Abaqus; see Table 7 and Section 6.2. In total there were 11 points (stresses p_c and strains $\epsilon_{\text{vol}}^{\text{pl}}$) given to Abaqus. These points are given the size of the yield surface on the $p-$ axes (where $q = 0$), as it is assumed that their is no shear q present during hydrostatic compression and plastic strain occurs as result of p_c only.

The elastic deformation it is in the Cam Clay model defined by the following parameters: E_{elastic} and ν_{elastic}:

- $E_{\text{elastic}} = 1 \cdot 10^9$ Pa. Since $\epsilon_{\text{in}}^{\text{pl}}$ is chosen very small this parameter the elastic region has negligible effect. However, no actual elastic behaviour could be measured in the performed experimental tests and thus no realistic value for this parameter was chosen.
- $\nu_{\text{elastic}} = 0.3$. No research is done for validation of this parameter.

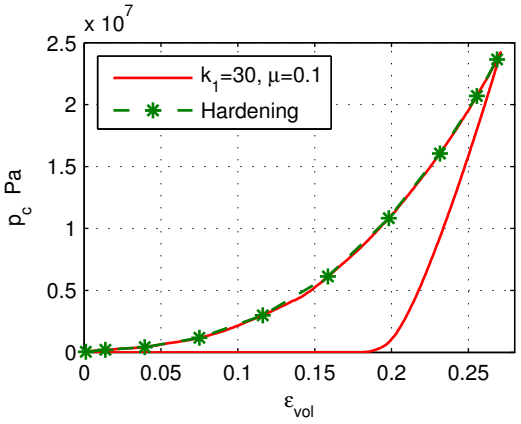

Figure 36: The hydrostatic pressure plotted versus volumetric strain during hydrostatic compression, for $k_1 = 30$, $\mu = 0.1$ and other model parameters given in Table 6. The hardening behaviour, described by the green asterisks, is given to Abaqus (p_c as function of $\epsilon_{\text{vol}}^{\text{pl}}$, see Table 7).

6.2 HYDROSTATIC COMPRESSION TESTS

During hydrostatic compression, or isotropic normal compression, the particle systems were pressurized in all directions, by very slowly moving the walls of the cuboidal system inwards with a sinusoidal velocity profile, with period $T = 50 \cdot \sqrt{\frac{1}{10^5}}$ s. The results of hydrostatic compression are shown in Figure 36; where the effective pressure $p_c = \frac{1}{3}(\sigma_1 + \sigma_2 + \sigma_3)$ are plotted against volumetric strain ϵ_{vol}; which can be regarded as plastic strain, since the elastic part is negligible. From the effective pressure 11 points (green asterisk) were chosen, the stresses and strains at these points were used as hardening data, see also Table 7.

6.3 TRIAXIAL TESTS

The principle behind a triaxial test is that the stress applied in the vertical direction can be different from the stresses applied in horizontal directions. In a homogeneous and isotropic material this produces a non-hydrostatic stress state, with shear stress that may lead to failure of the sample. In order to perform triaxial tests in this research, a sample was created by using the pressure control method as described in Section 4.2.3, ensuring that an equal starting pressure is acting on all walls. This was done for three different pressures: $p_{\text{ref}} = 6 \cdot 10^3$ Pa, $p_{\text{ref}} = 6 \cdot 10^4$ Pa and $p_{\text{ref}} = 6 \cdot 10^5$ Pa. When starting the triaxial tests, p_{ref} on the side walls was kept constant, the bottom wall was fixed, while the top wall moved downwards (strain-controlled). Because of the downwards movement the side walls are expanding to maintain the reference pressure. This explained setup conforms with true triaxial tests. For this case the effective pressure p (Equation 40) and Mises equivalent stress q (Equation 41) in terms of principal stresses are calculated:

Point	ϵ_{vol}^{pl}	p_c Pa
1	0.000	$5.084 \cdot 10^3$
2	0.007	$1.327 \cdot 10^5$
3	0.028	$3.202 \cdot 10^5$
4	0.061	$8.315 \cdot 10^5$
5	0.100	$2.161 \cdot 10^6$
6	0.143	$4.586 \cdot 10^6$
7	0.184	$8.934 \cdot 10^6$
8	0.220	$1.411 \cdot 10^7$
9	0.248	$1.907 \cdot 10^7$
10	0.265	$2.278 \cdot 10^7$
11	0.271	$2.418 \cdot 10^7$

Table 7: Hardening data obtained with hydrostatic compression performed with the use of DEM simulations. see Section 6.2.

$$p = 1/3\,(\sigma_1 + \sigma_2 + \sigma_3) = 1/3\,(\sigma_1 + 2\sigma_3) \tag{40}$$

$$\begin{aligned} q &= \sqrt{\frac{3}{2} S : S} = \sqrt{\frac{(\sigma_1 - \sigma_2)^2 + (\sigma_2 - \sigma_3)^2 + (\sigma_1 - \sigma_3)^2}{2}} \\ &= \sqrt{\frac{2\,(\sigma_1 - \sigma_2)^2}{2}} = \sigma_1 - \sigma_2 \end{aligned} \tag{41}$$

Note that $\sigma_1 = \sigma_2 = p_{ref}$ and σ_3 originates from the movement of the top wall. The results for different values of p_{ref} are plotted in Figures 37, 38 and 39. The tests with higher pressure show some better behaviour. Probably the system has problems in maintaining such a small reference pressure, although the average was conforming the other tests. It followed that:

$$M = \frac{q}{p} \approx 0.6 \tag{42}$$

6.4 IMPLEMENTATION IN ABAQUS

In Abaqus a cuboidal structure consisting of one element is created (linear cubic 3D Stress element). The side walls of this element were confined in x- and y-direction and the bottom wall is fully clamped. This element was loaded uniaxially by moving the top wall of the element downwards until the same strain level as in the DEM simulations is reached. In this research The "$k_1 = 30 \cdot 10^5$; $\mu = 0.1$" simulation, which best matches the oil-sample (see left bottom plot in Figure 26), was modelled in Abaqus with

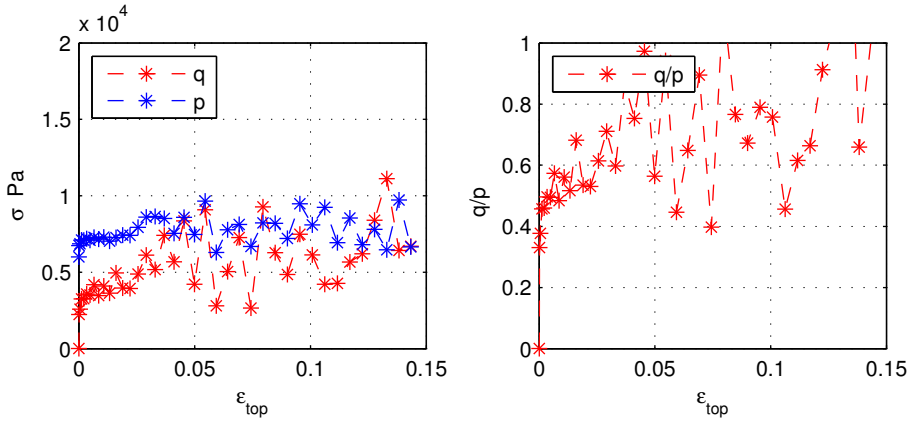

Figure 37: Results from triaxial analysis performed with the use of DEM simulations; $k_1 = 30 \cdot 10^5$, $\mu = 0.1$, $p_{\text{ref}} = 6 \cdot 10^3$ Pa and other model parameters are given in Table 6. First: the particle system were prepared with pressure control method (See section 4.2.3), so that an equal pressure (p_{ref}) on the walls of the cuboidal system was obtained (not shown in these plots). Then, the triaxial test was started by moving the top wall of the cuboidal system downwards, while p_{ref} was maintained on the side walls and the bottom wall was fixed. Left plot: p (defined in Equation 40) and q (defined in Equation 41) plotted versus top strain ϵ_{top} (the change in volume due to the top wall movement) during triaxial testing. Right plot: the ratio of q/p; this gives the critical state, if q/p becomes constant, the system is able to continue shearing to large strains without changing stresses or density.

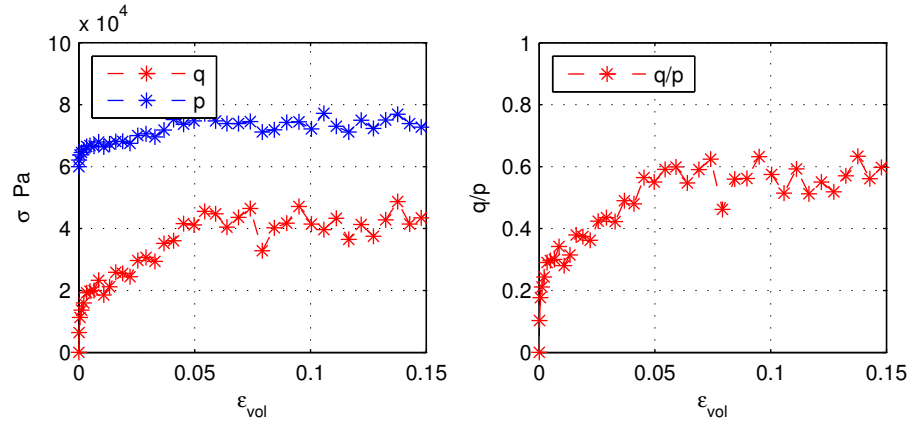

Figure 38: For explanation see the caption of Figure 37, note $p_{\text{ref}} = 6 \cdot 10^4$ Pa.

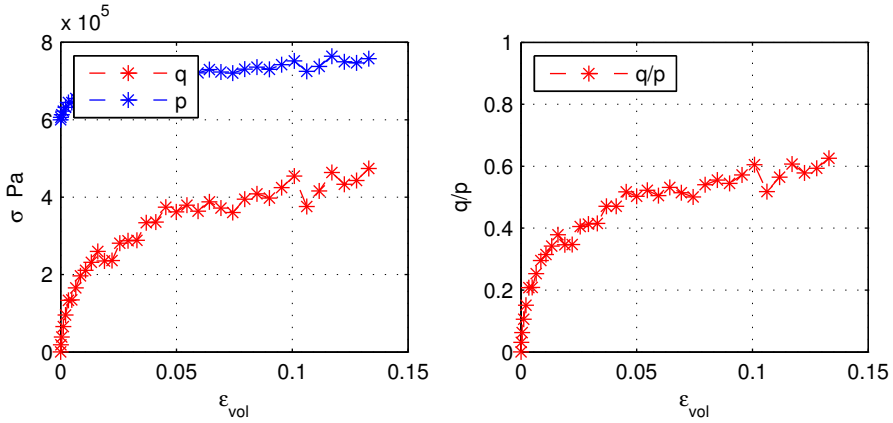

Figure 39: For explanation see the caption of Figure 37, note $p_{ref} = 6 \cdot 10^5$ Pa.

the Cam Clay material model. A parametric study of model parameters in this model has been performed, by varying M, β and K successively. The results are presented in Figure 40 and below explained:

- The top left plot with $M = 1$, $\beta = 1$ and $K = 1$ already shows a good agreement with the DEM simulation; as addition the experimental results of the bitumen-sample are also given, for which the DEM parameters were determined. This simulation is used as reference and in the following simulations M, β, and K are varied.
- In the top right plot, simulations with variable M, $\beta = 1$ and $K = 1$ were performed. From this plot can be seen that a higher M parameter is leading to higher stresses, this seems logical, because if M becomes higher then the yield locus (height) becomes larger at equal levels of p (assuming $q \neq 0$). Resulting in higher stresses in the stress-strain curves.
- In the bottom left plot, simulations with variable β were performed, while $M = 1$ and $K = 1$. It followed that a decrease in β is leading to an increase in stress. This parameter influences the size of the yield surface a, see equation 39, and the shape on the wet side of the yield surface (see Figure 35). To ensure the correct position of p_c (defined by the hardening data; see Table 7) on the pressure axis ($t = 0$) the yield surface will be scaled upwards with a lower β. Consequently, higher pressure will be reached, resulting in higher stresses in the stress-strain curves.
- In the bottom right plot, the effects of variable K are shown. It appears that this parameter has no effect in the simulations, because the same stress path is followed during compaction.

From the triaxial tests it can be concluded that $M \approx 0.6$. This value for M even improves the fit between Abaqus and DEM simulations; see Figure 41. The unloading is dependent on the modulus of the elastic part E_{elastic}, this is shown in Figure 42. Here can be seen that E_{elastic} determines the

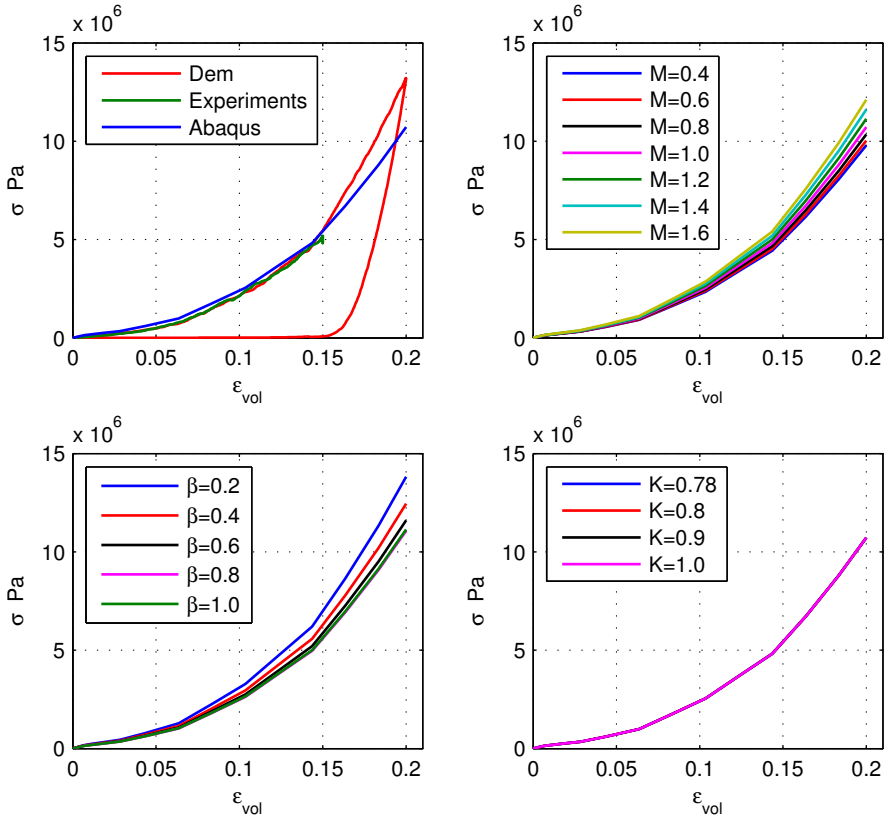

Figure 40: Stress-strain relations obtained with Abaqus simulations compared with results from DEM and experiments. The effect of different Abaqus parameters was investigated (M, β and K; see the legends), for a detailed explanation see Section 6.4.

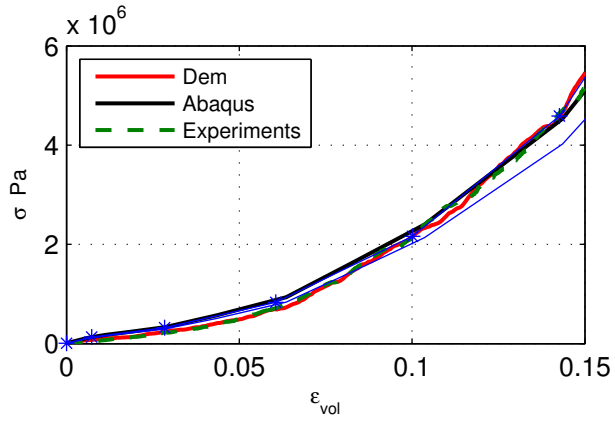

Figure 41: Stress-strain relations obtained with: Abaqus, DEM and experiments. The calculated value for $M = 0.6$, with use of triaxial rests, increases the fit between Abaqus and DEM.

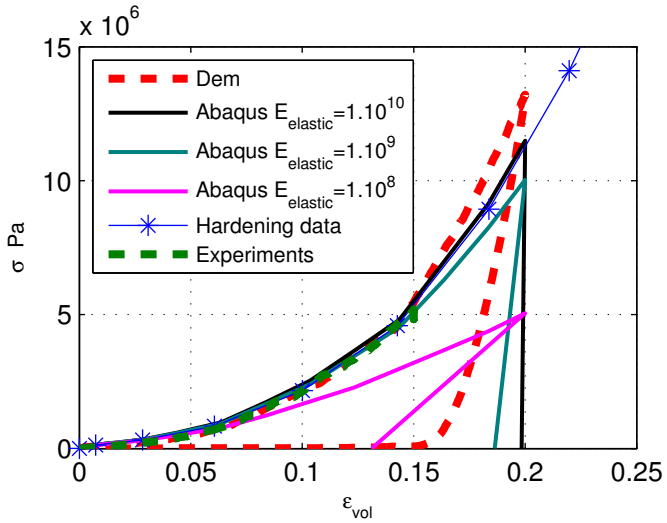

Figure 42: In this simulation the influence of E_{elasctic} is investigated; E_{elastic} affects the unloading; see the different slopes during unloading for variable E_{elastic} and the loading; probably, the plastic deformation consists of an elastic- and plastic part; where E_{elastic} affects the elastic part

slope during unloading and thus the amount of plastic deformation. Furthermore it followed that E_{elastic} also affects the loading behaviour. Probably, the hardening behaviour consists of an elastic- and plastic part; where E_{elastic} affects the elastic part. The stress levels in Abaqus deviate for large strain levels $\epsilon_{\text{vol}} > 0.15$, from the DEM simulations. This seems logical, because uniaxial compaction deviates from hydrostatic compression, especially for large strain levels the stress in uniaxial compaction will be higher.

6.5 CONCLUSIONS

- The DEM model is successfully linked to a continuum model applicable on the macro-scale. The yield locus for different strain levels was defined by hardening data $p_c\left(\epsilon_{\text{vol}}^{\text{pl}}\right)$, obtained by a hydrostatic compression test, performed with the use of DEM simulations.
- The slope of the critical state line (parameter M) was obtained with triaxial tests, performed with the use of DEM simulations.
- The hardening data is strongly determining the behaviour during compaction. The influence of M is low, because changing this parameter affects the stress-strain curves barely, so it can be concluded that there is not much shear (q) present in uniaxial compaction.
- The results between Abaqus and DEM are in good agreement for strain levels $\epsilon_{\text{vol}} < 0.15$.
- For larger strain levels $\epsilon_{\text{vol}} > 0.15$, the uniaxial compaction results from the Abaqus simulation differ from the DEM-simulations.

- The amount of plastic deformation (visible after unloading) is depending on E_{elastic}; this is the slope during unloading in the stress-strain curves. Unfortunately, no realistic value for this parameter was obtained in this research.
- E_{elastic} also influences the slope during loading. Probably, the hardening behaviour consists of an elastic- and plastic part; where E_{elastic} affects the elastic part. This has to be taken into account in future research.

7 CONCLUSIONS AND RECOMMENDATIONS

This is the final chapter of the thesis. First, a summary of the performed work is given in Section 7.1. Then, the most important conclusions are summed up (in Section 7.2). The chapter concludes with recommendations for future research in Section 7.3.

7.1 SUMMARY

Nowadays, compaction is an important topic and a numerical model capable of describing compaction, can contribute to a better understanding of the compaction process, which is useful for constructing better better roads. However, fundamental micro-based numerical models, capable of describing asphalt compaction behaviour on the macro-scale, are not available. In this research a meso-scale model, suitable for modelling the meso-scale behaviour of particles using micro-based parameters, has been developed and calibrated. This model has been linked to a continuum model, which made modelling on the macro-scale possible.

For simplicity reasons, a simplified method of compaction has been considered, because realistic compaction (performed by rollers or in laboratory tests), is too difficult to model. This simplified method of compaction is called uniaxial compaction, where compaction is realized under influence of a uniaxial load.

No similar uniaxial compaction tests were known; therefore, it was uncertain whether this method would actually lead to compaction or not. This has been investigated in the laboratory where uniaxial compaction tests on actual asphalt mixtures were performed. The results were promising: the density of the compacted samples differed only slightly from conventional compaction tests. However, as from stress-levels of approximately $2 \cdot 10^5$ Pa, particle crushing occurred, which is unwanted during compaction.

With the use of DEM, a model was developed capable of describing the behaviour during experimental compaction. For this purpose, the non-compacted state of the asphalt mixture was created in DEM (during the so called preparation step) and compaction was carried out in another DEM simulation. It appeared that the preparation step strongly affected the compaction simulation and showed interesting effects of micro-based model parameters on the macroscopic behaviour. Nevertheless, this is undesirable if a model is wanted capable of modelling compaction experiments, what was the main goal of the research. For this reason, it was chosen to create equally strong samples during preparation.

The compaction simulations were compared with the results of the experimental tests in which an open asphalt mixture was compacted. In order to relate model properties to physical aspects of the asphalt, two different

bitumen were used in these tests: (1) a hot bitumen and (2) a fake bitumen (lubrication oil). It followed that by adapting the k_1 parameter in the DEM contact model, the different types of bitumen could be modelled quantitatively.

Finally, the developed DEM model was linked to a continuum model that can be applied on the macro-scale. For this purpose the Cam Clay material model available in Abaqus (FEM program) has been chosen, because it can handle large deformations and it is possible to dictate the hardening behaviour. To calibrate this model, tests are needed which describe the hardening behaviour and the model parameters. Two types of calibration tests have been performed with the use of DEM simulations: (1) hydrostatic compression tests and (2) triaxial tests. With the use of the hydrostatic compression tests the hardening behaviour has been defined piecewise, and from the triaxial tests the slope of the critical state line was derived.

Next, parameters were used in a simple one-element structure in Abaqus, to which similar loading and boundary conditions as in the DEM simulations and experimental tests were applied. The results were presented in stress-strain relations and compared with the experimental and DEM simulations. A good quantitative agreement between FEM, DEM and experiments was obtained.

At first glance, this analysis seems superfluous: why perform two calibration simulations in DEM in order to define parameters for a macro-scale model? However, once the micro- and meso-based properties have been defined in FEM, it becomes easy to expand the model to larger scales, for example by adding more elements with the same material behaviour as obtained in DEM. This approach makes modelling on a macro-scale using micro- and meso-based parameters feasible. If a DEM model can be created which describes the behaviour of asphalt mixtures under realistic compaction loading, for example loading applied by rollers, and if the material behaviour is introduced in FEM, it should be possible to simulate actual compaction as performed by rollers with micro-based parameters. This is the ambitious goal for future research.

7.2 CONCLUSIONS

- Applying an uniaxial load on non-compacted asphalt mixtures leads to a compacted sample. It appeared that the density of this compacted sample was approaching the density obtained in conventional compaction tests; particle crushing occurred as from stress levels of approximately $\sigma \geqq 2 \cdot 10^5$ Pa (not explicitly modeled in DEM).

- A meso-model based on DEM, capable of modelling uniaxial compaction has successfully been developed and calibrated with experiments. Two different kind of simulations were performed: (1) the creation of a non-compacted, solid, isotropic, random particle system

and (2) the uniaxial compaction simulation. The preparation procedure and choice of parameters, can affect the compaction simulation.

- To obtain a well defined initial strength, constant friction was used during preparation and samples were exerting a constant pressure on the walls of the cuboidal volume, which conforms with the initial pressure in the experiments, while the volume fraction differed.
- The results of the compaction were presented in stress-strain curves; these were in good agreement with the experimental tests. By treating both mastic and aggregate as one spherical particle, the modelling is greatly simplified, without losing the meso-structure and the restructuring capabilities of the aggregates.
- With the use of the elasto-plastic contact model, the bitumen in the mastic can be modelled, by only varying the stiffness parameter k_1.
- With the friction parameter μ the curve can be proportionally scaled over the whole stress-strain curve. It is not possible to relate this parameter directly to internal friction in the asphalt mixture.
- Reducing friction is leading to better compaction, because occurring stress levels are lower and less elastic recovery after unloading is present.
- In the performed simulations the influence of k_2 was small; not many contacts occurred in the elastic region of the contact model.
- A macro-scale model was obtained by using results from the DEM model to calibrate the FEM model (Abaqus). For this purpose an existing material model was chosen (Cam Clay model). To calibrate this model 2 types of tests have been performed with the use of DEM simulations: (1) a hydrostatic compression test and (2) a triaxial test.
- With the hydrostatic compression test the hardening behaviour was dictated, this strongly determined the behaviour during compaction. However for larger strain levels $\epsilon_{\text{vol}} > 0.15$, the hardening behaviour differed from the compaction behaviour.
- With the triaxial tests the slope of the critical state line was determined (M, the ratio of q to p at critical state) and used as model parameter in the Cam Clay material model. However, the influence of M turned out to be small during uniaxial compaction.

7.3 RECOMMENDATIONS

- Perform compaction tests in DEM and in practice where more shearing is present. This will probably lead to a better compacted sample and it can be ascertained whether the defined model parameters are correct or not.

- Try to capture the unloading of uniaxial asphalt compaction in experimental tests; these results will provide data for determining the k_2 model parameter in DEM and E_{elastic} in Abaqus
- The reproducibility of the DEM simulation has not been investigated. Different starting velocities and positions in DEM preparation simulations may lead to a somewhat different structure and compaction results.
- The reproducibility of the experiments has not been investigated. A slightly different preparation method may lead to somewhat different results.
- In all compaction tests and simulations confined boundaries were used (except the top wall). In reality this will not be the case; this has to been taken into account when creating a more realistic model.
- The gradation of particle sizes in DEM was not exactly conform the experiments; however, good results were nevertheless obtained. It would be interesting to see if the effect of gradation can be noticed in stress-strain curves. If so, relations between gradation and compaction can be made.
- During preparation a constant friction $\mu = 0.2$ was chosen; this might underestimate the compaction simulations where $\mu = 0.1$, because it followed that lower friction was leading to denser samples during preparation. Therefore, the sample with $\mu = 0.1$ is relatively weaker than the other samples. Therefore, it may be wiser to use a constant friction coefficient of $\mu = 0.1$.
- The influence of k_t is not studied during preparation, this might affect the creation of the solid state.
- The behaviour for different μ, might resemble the expected behaviour when temperature changes.
- In the performed simulations the influence of k_2 was small; not many contacts occurred with this stiffness. If this does not conform to realistic conditions, a smaller plasticity range (defined by parameter ϕ) should be used. The k_2 regime will then be reached earlier.
- The plasticity range parameter ϕ was based on the average particle size and during the calculation the pre-factor (see Section 2.5 was ignored). This parameter is very important, it represents physically the amount of mastic and numerically the transits to k_2^*, which will definitely be of great influence during compaction. The calculation of the ϕ parameter based on all particles and k_2^* would be more consistent.
- Improve the pressure control method, so that an isotropic structure is obtained during the wall movement mode, because this is the most easiest way to define a proper initial state.

- In this research a solid system is assumed necessary after preparation. This constraints the preparation method, maybe with a non-solid state even better results can be obtained.
- Try to capture the behaviour of actual compaction (compaction by rollers, or gyrator tests) in DEM and use this in a FEM program on the macro-scale in order to build a realistic model of compaction. This is the ambitious goal of future research.

APPENDIX

A

PROPERTIES "FAKE BITUMEN" (OR LUBRICATION OIL)

REGENIS® 50 FLUID

BITUMEN VOOR HERGEBRUIK

Waarden		TEST METHODE	SPECIFICATIE	TYPICALS
Dichtheid bij 15°C	Kg/m^3	***EN ISO 12185***	940 - 1010	**994.4**
Kinematische Viscositeit bij 100 °C	mm^2/s	EN ISO 3104	50 - 85	**71.4**
Vlampunt (Cleveland)	°C	EN ISO 2592	≥ 230	**300**
Minimum verpompbaarheids temperatuur (viscositeit van 15 poises)	°C	-	30	**45**
Verlies van massa bij verhitting gedurende 5h bij 163°C	%	NF T 66-011	≤ 2	**<2**

Geproduceerd en beschikbaar op: **Refinaderij Normandië**

Voor alle **REGENIS® bitumen** geldt een levertijd in overleg.

SAFETY DATA SHEET

REGENIS® 50 safety data sheet is beschikbaar op de website www.quickfds.com.

2 januari 2008
TOTAL Nederland N.V.
Nieuwe Havenstraat 2
NL - 2272 AD Voorburg

BIBLIOGRAPHY

[1] *Critical State (Clay) Plasticity Modeling, Section 22.3.4 Abaqus manual*. (Cited on page 63.)

[2] D. Little H. Zbib E. Masad *, L. Tashman. Viscoplastic modeling of asphalt mixes with the effects of anisotropy, damage and aggregate characteristics. *Mechanics of Materials*, 37:1242–1256, 2007. (Cited on page 3.)

[3] W. G. Buttlar H. Kim *. Discrete fracture modeling of asphalt concrete. *International Journal of Solids and Structures*, 46:2593–2604, 2009. (Cited on pages 3 and 4.)

[4] W. G. Buttlar H. Kim, M.P. Wagoner. Micromechanical fracture modeling of asphalt concrete using a single-edge notched beam test. *Materials and Structures*, 42:677–689, 2009. (Cited on pages 3 and 4.)

[5] Shihui Shen * Huanan Yu. Impact of aggregate packing on dynamic modulus of hot mix asphalt mixtures using three-dimensional discrete element method. *Construction and Building Material*, 26:302–309, 2012. (Cited on pages 3 and 4.)

[6] D. Little H. Zbib L. Tashman, E.Masad. A microstrucure-based viscoplastic model for asphal concrete. *International Journal of Plasticity*, 21:1659–1685, 2005. (Cited on page 5.)

[7] S.P. Wu A.A.A. Molenaar L.T. Mo, M. Huurman. Investigation into stress states in porous asphalt concrete on the basis of fe-modeling. *Finite elements in Analysis and Design*, 43:333–343, 2007. (Cited on page 4.)

[8] S.P. Wu A.A.A. Molenaar L.T. Mo, M.Huurman. 2d and 3d meso-scale finite element models for ravelling analysis of porous asphalt concrete. *Finite Elements in Analysis and Design*, 44:186–196, 2008. (Cited on page 4.)

[9] S. Luding. Introduction to discrete element methods. *EJECE*, 12:785–826, 2008. (Cited on pages 6, 17, 20, and 21.)

[10] S. Luding. Cohesive, frictional powders: contact models for tension. *Granular Matter*, 10:235–246, 2008. (Cited on page 17.)

[11] Q. Dai M. H. Sadd *. A comparison of micro-mechanical modeling of asphalt materials using finite elements and doublet mechanics. *Mechanics of Materials*, 37:641–662, 2005. (Cited on page 3.)

[12] M.F. Woldekidan R.N. Khedoe J.Moraal M. Huurman, L. Mo. Overview of the lot meso mechanical research into porous asphalt raveling. 2009. (Cited on page 4.)

[13] M.F.C van de Ven P.M Muraya, A.A.A. Molenaar. Contribution of the nituminous mortar and stone skeleton to the resistance to permanent deformation in asphalt mixtures. *Journal of testing and evaluation*, 537, 2009. (Cited on page 5.)

[14] Z. You Q. Dai. Prediction of creep stiffness of asphalt mixture with micromechanical finite-element and discrete-element models. *Journal of Engineering Mechanics ASCE*, February 2007. (Cited on page 3.)

[15] R. Kim T. Yun. Modeling of viscoplastic rate dependent hardening-softening behaviour of hot mix asphalt in compression. *Mech Time-Depend Mater*, 15:89–103, 2011. (Cited on page 5.)

[16] H.L. ter Huerne. *Compaction of Asphalt Road Pavements*. PhD thesis, University of Twente, 2004. (Cited on page 4.)

[17] S. Luding. V. Magnanimo*, H. L. ter Huerne. Modeling of asphalt durability and self-healing with discrete particle method. 2012. (Cited on page 17.)

[18] D. M. Wood. *Soil Behaviour and Critical State Soil Mechanics*. Cambridge University Press, 1990. (Cited on page 63.)

[19] Z. You Y. Liu. Visualization and simulation of asphalt concrete with randomly generated three-dimensional models. *Journal of computing in civil engineering ASCE*, November/December 2009, 2009. (Cited on page 3.)

[20] Q. Dai Z. You. Review of advances in micromechanical modeli of aggregate interactions in asphalt mixtures. *Canadian Journal of Civil Engineering*, 34:239–252, 2007. (Cited on pages 3 and 4.)

[21] Q. Dai Z. You, S. Adhikari. Three-dimensional discrete element models for asphalt mixtures. *Journal of Engineering Mechanics ASCE*, December 2008. (Cited on pages 3 and 4.)